Shadowing and Small x Physics on J/ψ Production at RHIC

R. Vogt

Nuclear Science Division, Lawrence Berkeley National Laboratory, Berkeley, CA 94720, USA

Physics Department, University of California, Davis, CA 95616, USA

Outline

- Color Evaporation Model

- Setting the Parameters from Heavy Flavor Production

- J/ψ Production in pp, d+Au and AA Collisions at RHIC

- Initial and Final State Effects

Calculating Heavy Flavors in Perturbative QCD

'Hard' processes have a large scale in the calculation that makes perturbative QCD applicable: high momentum transfer, μ^2, high mass, m, high transverse momentum, p_T, since $m \neq 0$, heavy quark production is a 'hard' process

Asymptotic freedom assumed to calculate the interactions between two hadrons on the quark/gluon level but the confinement scale determines the probability of finding the interacting parton in the initial hadron

Factorization assumed between the perturbative hard part and the universal, nonperturbative parton distribution functions

The hadronic cross section in an AB collision where $AB = pp, pA$ or nucleus-nucleus is

$$\sigma_{AB}(S, m^2) = \sum_{i,j=q,\overline{q},g} \int_{4m_Q^2/s}^{1} \frac{d\tau}{\tau} \int dx_1 \, dx_2 \, \delta(x_1 x_2 - \tau)$$
$$\times f_i^A(x_1, \mu_F^2) \, f_j^B(x_2, \mu_F^2) \, \widehat{\sigma}_{ij}(s, m^2, \mu_F^2, \mu_R^2)$$

f_i^A are the nonperturbative parton distributions, determined from fits to data, x_1 and x_2 are the fractional momentum of hadrons A and B carried by partons i and j, $\tau = s/S$

$\widehat{\sigma}_{ij}(s, m^2, \mu_F^2, \mu_R^2)$ is hard partonic cross section calculable in QCD in powers of α_s^{2+n}: leading order (LO), $n = 0$; next-to-leading order (NLO), $n = 1$ ...

Results depend strongly on quark mass, m, factorization scale, μ_F, in the parton densities and renormalization scale, μ_R, in α_s

2

Quarkonium Production: Color Evaporation Model (CEM)

All quarkonium states are treated like $Q\overline{Q}$ below $H\overline{H}$ threshold

Distributions (x_F, p_T, $\sqrt{s}$, A) for all quarkonium family members identical — leads to constant ratios

At LO, $gg \to Q\overline{Q}$ and $q\overline{q} \to Q\overline{Q}$; NLO add $gq \to Q\overline{Q}q$

$$\sigma_C^{\rm CEM} = F_C \sum_{i,j} \int_{4m^2}^{4m_H^2} d\hat{s} \int dx_1 dx_2 \; f_{i/p}(x_1, \mu^2) \; f_{j/p}(x_2, \mu^2) \; \hat{\sigma}_{ij}(\hat{s}) \; \delta(\hat{s} - x_1 x_2 s)$$

F_C fixed at NLO from total cross section data as a function of $\sqrt{s}$, $\sigma(x_F > 0)$ for inclusive J/ψ and $B_{\mu\mu} d\sigma(\Upsilon + \Upsilon' + \Upsilon'')_{y=0}/dy$

Values of m and μ (here $\mu \propto \sqrt{(p_{TQ}^2 + p_{T\overline{Q}}^2)/2 + m_Q^2} = m_{TQ\overline{Q}} \equiv m_T$ in the exclusive $Q\overline{Q}$ code) for several parton densities fixed from $Q\overline{Q}$ production, as described in the following

$\chi_c/J/\psi$ Ratio Energy Independent

HERA-B plot comparing $R_{\chi c} = \sigma(\chi_c)/\sigma(J/\psi)$ with πA and pA data

Color singlet model (CSM) result is high since direct J/ψ only comes from $gg \to J/\psi g$, a 4-point vertex at $\mathcal{O}(\alpha_s^3)$, while χ_c is produced at $\mathcal{O}(\alpha_s^2)$ by $gg \to \chi_c$

Nonrelativistic QCD (NRQCD) is lower, especially at low energies, because of greater importance of $q\bar{q} \to \chi_c X$ channel, the octet contribution where octet J/ψ matrix element is much bigger

Result is most consistent with $R_{\chi c}$ independent of $\sqrt{S}$, as predicted by CEM

CDF result, $R_{\chi c} = 0.297 \pm 0.017 \pm 0.057$, consistent with fixed-target results
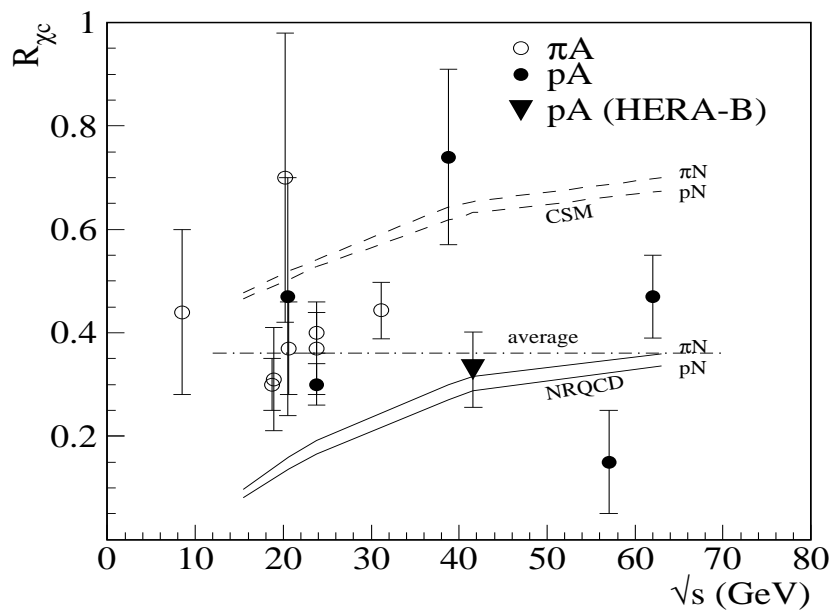

Figure 1: Ratio of χ_c to J/ψ cross sections as a function of $\sqrt{S}$ for πA and pA fixed-target measurements. The CSM and NRQCD curves are obtained from Monte Carlo while the 'average' is the average value of all measurements. From I. Abt *et al.* (HERA-B Collab.), Phys. Lett. **561** (2003) 61.

4

$\psi'/J/\psi$ Ratio Also Energy Independent

Data are from pp and pA interactions
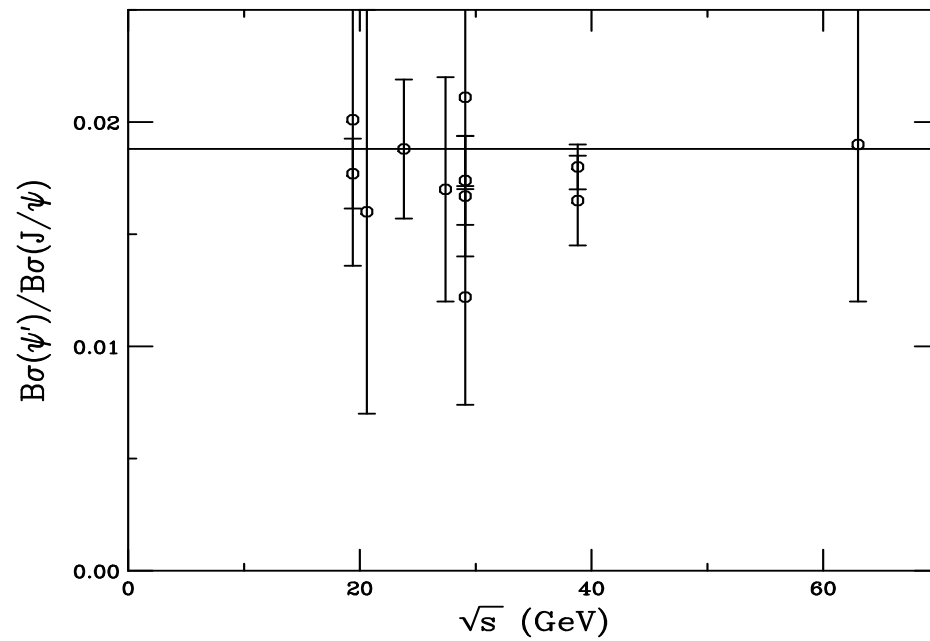
Solid curve corresponds to CEM

Figure 2: Ratio of ψ' to J/ψ cross sections with lepton pair branching ratios included as a function of $\sqrt{S}$ for pp and pA measurements. Adapted from R.V., Phys. Rept. **310** (1999) 197.

5

Production and Feeddown Fractions

.

Data and branching ratios can be used to separate out the F_C's for each state in quarkonium family

Resonance	$\sigma_i^{\text{dir}}/\sigma_H$	f_i
J/ψ	0.62	0.62
ψ'	0.14	0.08
χ_{c1}	0.6	0.16
χ_{c2}	0.99	0.14
Υ	0.52	0.52
Υ'	0.33	0.10
Υ''	0.20	0.02
$\chi_b(1P)$	1.08	0.26
$\chi_b(2P)$	0.84	0.10

Table 1: The ratios of the direct quarkonium production cross sections, σ_i^{dir}, to the inclusive J/ψ and Υ cross sections, denoted σ_H, and the feed down contributions of all states to the J/ψ and Υ cross sections, f_i.

Calculating Heavy Flavor Total Cross Sections

Partonic total cross section only depends on quark mass m, not kinematic quantities

To NLO

$$\hat{\sigma}_{ij}(s, m, \mu_F^2, \mu_R^2) = \frac{\alpha_s^2(\mu_R^2)}{m^2} \Big\{ f_{ij}^{(0,0)}(\rho)$$
$$+ \ 4\pi\alpha_s(\mu_R^2) \left[f_{ij}^{(1,0)}(\rho) + f_{ij}^{(1,1)}(\rho) \ln(\mu_F^2/m^2) \right] + \mathcal{O}(\alpha_s^2) \Big\}$$

$\rho = 4m^2/s$, s is partonic center of mass energy squared

μ_F is factorization scale, separates hard part from nonperturbative part

μ_R is renormalization scale, scale at which strong coupling constant α_s is evaluated

$\mu_F = \mu_R$ in evaluations of parton densities

$f_{ij}^{(a,b)}$ are dimensionless, μ-independent scaling functions, $a = 0$, $b = 0$ and $ij = q\bar{q}$, gg for LO, $a = 1$, $b = 0, 1$ and $ij = q\bar{q}$, gg and qg, $\bar{q}g$ for NLO

$f_{ij}^{(0,0)}$ are always positive, $f_{ij}^{(1,b)}$ can be negative also

Note that if $\mu_F^2 = m^2$, $f_{ij}^{(1,1)}$ does not contribute

Scaling Functions to NLO

Near threshold, $\sqrt{s}/2m \to 1$, Born contribution is large but dies away for $\sqrt{s}/2m \to \infty$

At large $\sqrt{s}/2m$, gg channel is dominant, then qg

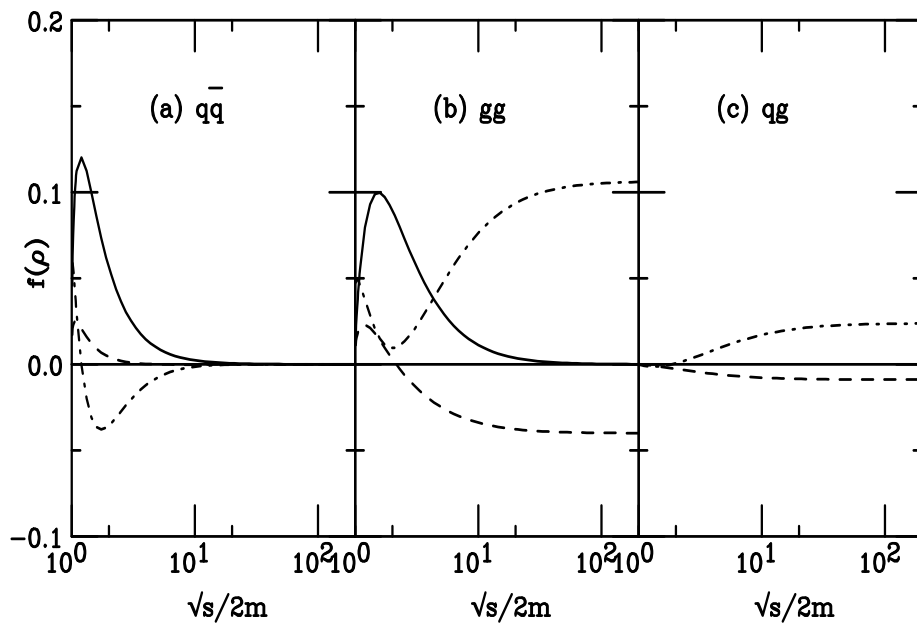High energy behavior of the cross sections due to phase space and low x behavior of parton densities

Figure 3: Scaling functions needed to calculate the total partonic $Q\overline{Q}$ cross section. The solid curves are the Born results, $f_{ij}^{(0,0)}$, the dashed and dot-dashed curves are NLO contributions, $f_{ij}^{(1,1)}$ and $f_{ij}^{(1,0)}$ respectively.

Comparison of $c\bar{c}$ Calculations to Data

Two ways to evaluate total cross sections and make predictions for higher energies

There are only 2 important parameters at fixed target energies: the quark mass m and the scale μ – at higher energies, the low x, low μ behavior of the parton densities plays an important role in the asymptotic result

The scale is usually chosen so that $\mu_F = \mu_R$, as in parton density fits although there is no strict reason for doing so for heavy flavors

First way (RV, Hard Probes Collaboration): fix m and $\mu \equiv \mu_F = \mu_R \geq m$ to data at lower energies and extrapolate to unknown regions – tends to favor lower masses

Second way (Cacciari, Nason and RV): determine an uncertainty band within $1.3 < m < 1.7$ GeV for charm and $4.5 < m < 5$ GeV for bottom with $(\mu_F/m, \mu_R/m) = (1, 1)$, (2,2), (0.5,0.5), (0.5,1), (1,0.5), (1,2), (2,1)

We have to be careful with the resulting total charm cross sections for $\mu_F \leq m$ with the CTEQ6M parton densities since the minimum μ is 1.3 GeV, giving us big K factors for the lower scales and making the use of $\mu_F \leq m$ problematic, to say the least!

Densities like GRV98 have a lower starting scale, making their behavior for low x, low μ charm production less problematic

Note also that even the two-loop evaluation of α_s is big for low scales, for $m = 1.5$ GeV: $\alpha_s(m/2 = 0.75) = 0.648$, $\alpha_s(m = 1.5) = 0.348$ and $\alpha_s(2m = 3) = 0.246$

CTEQ6M Densities at $\mu = m/2$, m and $2m$

CTEQ6M densities extrapolate to $\mu < \mu_{\min} = 1.3$ GeV

When backwards extrapolation leads to $xg(x, \mu) < 0$, then $xg(x, \mu) \equiv 0$
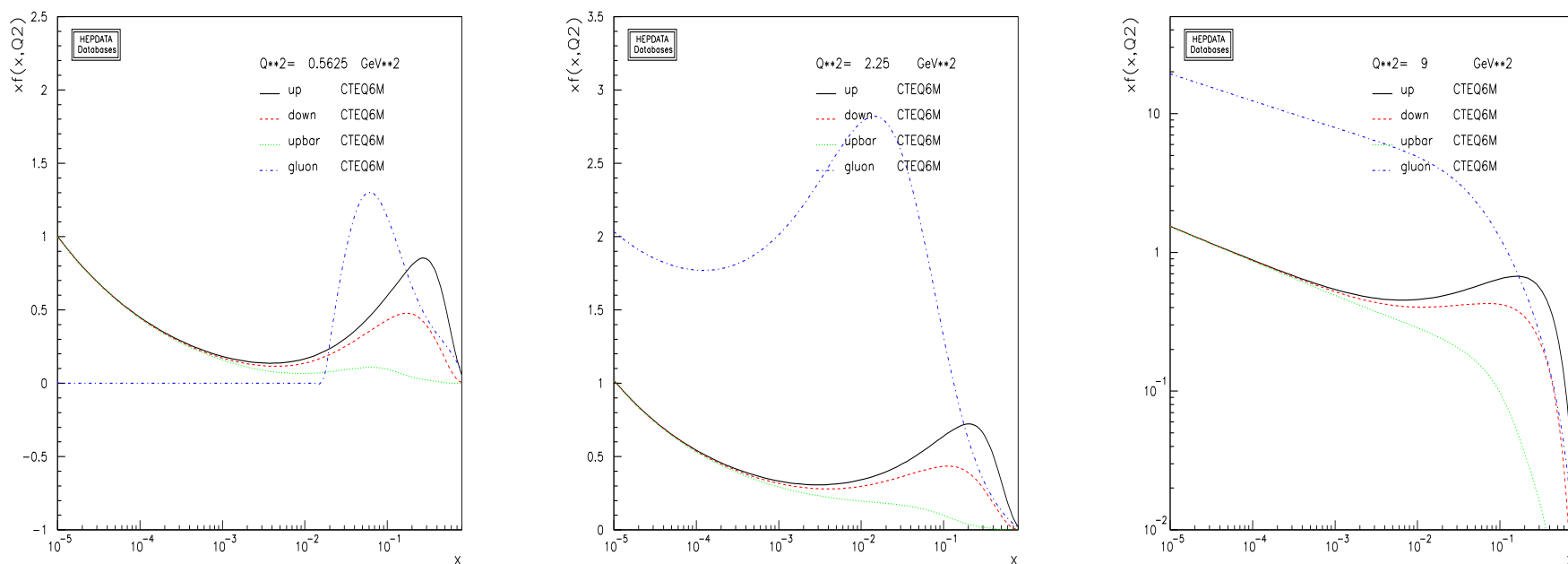

Figure 4: The CTEQ6M parton densities as a function of x for $\mu = m/2$ (left), $\mu = m$ (middle) and $\mu = 2m$ (right) for $m = 1.5$ GeV.

Fixing m and μ^2 to All Data: Method 1

Difficult to obtain a large calculated $c\bar{c}$ cross section with $\mu_F^2 = \mu_R^2$, as in parton density fits

Data favors lower masses – lowest mass used here is 1.2 GeV but much lower masses than allowed in pQCD needed to agree with largest cross sections
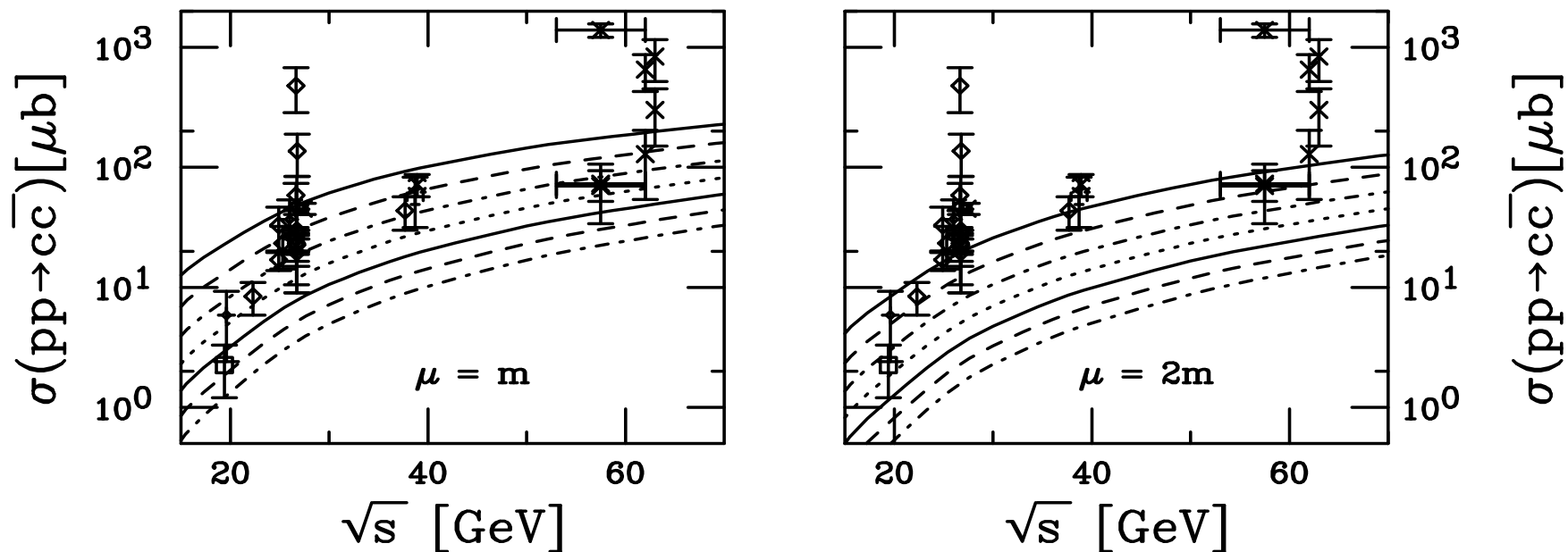

Figure 5: Total $c\bar{c}$ cross sections in pp and pA interactions up to ISR energies as a function of the charm quark mass using the CTEQ6M parton densities. The left-hand plot shows the results with $\mu_F = \mu_R = m$ while in the right-hand plot $\mu_F = \mu_R = 2m$. From top to bottom the curves are $m = 1.2$, 1.3, 1.4, 1.5, 1.6, 1.7, and 1.8 GeV.

Extrapolation to Higher Energies

We have kept only the most recent measurements, including the PHENIX $\sqrt{S} = 130$ GeV result from Au+Au, lowest $\sqrt{S} = 200$ GeV point is from PHENIX pp

Note the $\mu = m$ behavior at high energy: the cross section grows slower with $\sqrt{s}$ due to the small x behavior of $xg(x, \mu)$ for μ close to $\mu_{\min}$
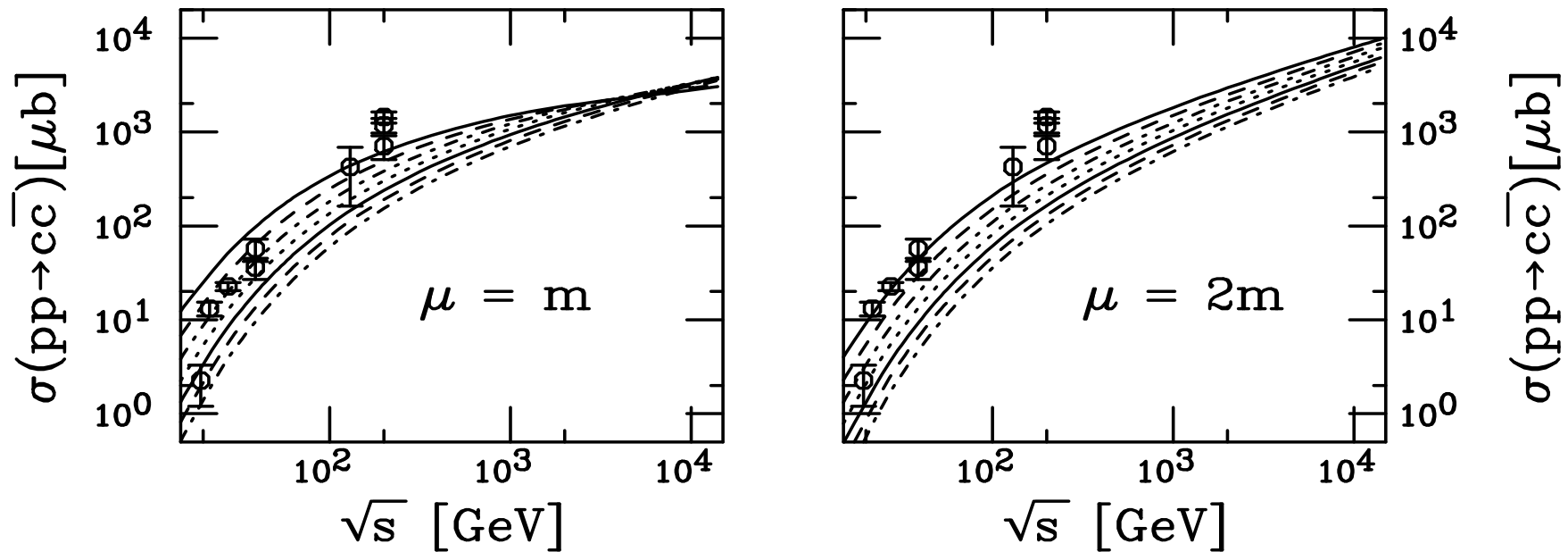

Figure 6: Same as previous but the energy range extended to LHC energies.

K Factors Using Method 1

K factors defined here as the ratio of the NLO to LO cross sections, both calculated with NLO parton densities and two loop evaluation of α_s

Note the $\mu = m$ behavior at high energy – K factors grow at low mass and then turn over due to both the low x parton densities and the fact that the LO cross section gets small far from threshold

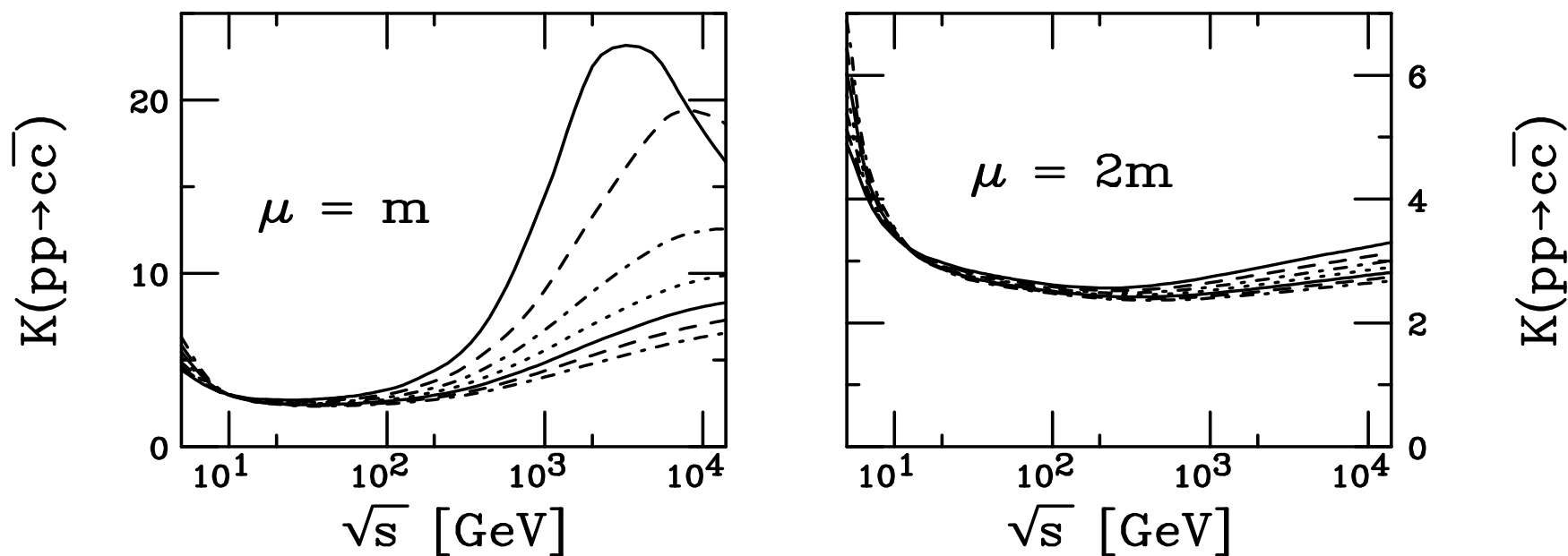The larger the value of μ, the better behaved the K factors

Figure 7: The K factors over the full $\sqrt{s}$ range.

Theoretical Uncertainty Band: Method 2

Curves with $(\mu_F/m, \mu_R/m) = (1, 0.5)$ and $(0.5, 0.5)$ have large total cross sections since $\alpha_s(m/2) = 0.648$, really too high to get a convergent result

Curves with $\mu_F \leq m$ turn over for $\sqrt{s} > 100$ GeV due to low x, low μ behavior of parton densities
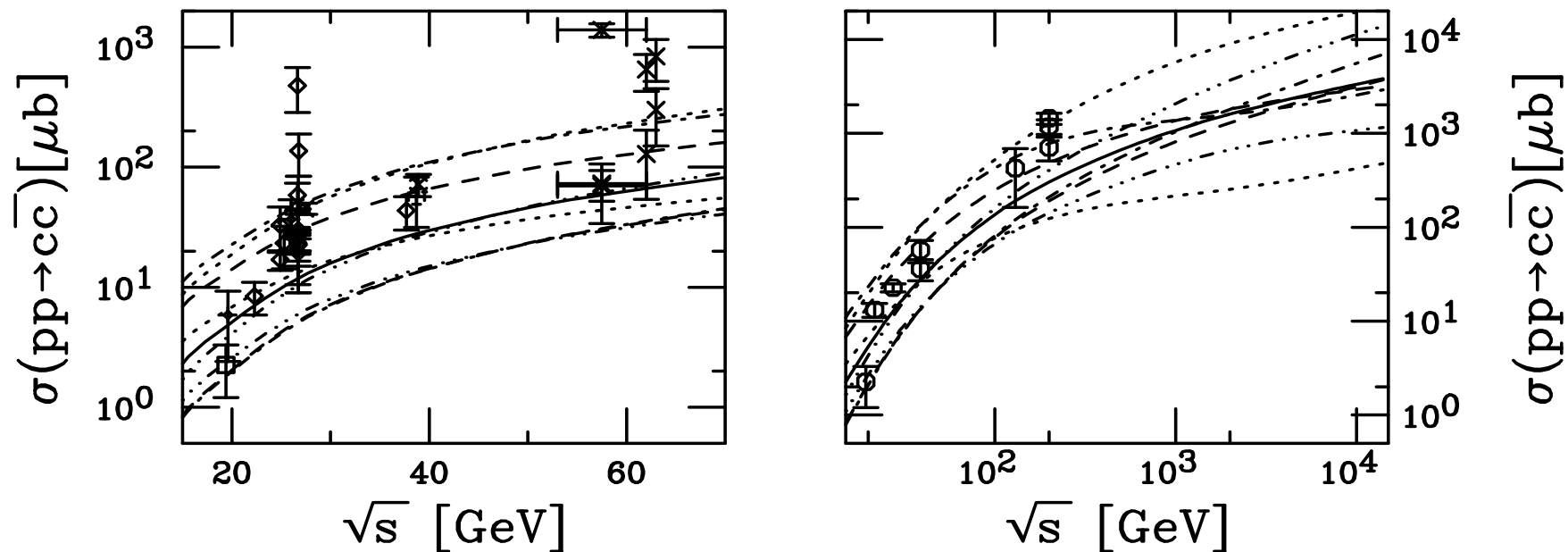

Figure 8: Total $c\bar{c}$ cross sections calculated using CTEQ6M. The solid curve is the central value $(\mu_F/m, \mu_R/m) = (1, 1)$ with $m = 1.5$ GeV. The upper and lower dashed curves are $m = 1.3$ and 1.7 GeV with $(1,1)$ respectively. The upper and lower dot-dashed curves correspond to $(0.5, 0.5)$ and $(2, 2)$ while the upper and lower dotted curves are with $(1, 0.5)$ and $(0.5, 1)$ with $m = 1.5$ GeV.

Theoretical Uncertainty Band: K Factors

Results with $(\mu_F/m, \mu_R/m) = (1, 0.5)$ and $(0.5, 0.5)$ have largest K factors

Results with $(1,1)$, $(2,2)$, $(2,1)$ and $(1,2)$ with $m = 1.5$ GeV and $(1,1)$ with $m = 1.7$ GeV give $K < 10$ at highest energies
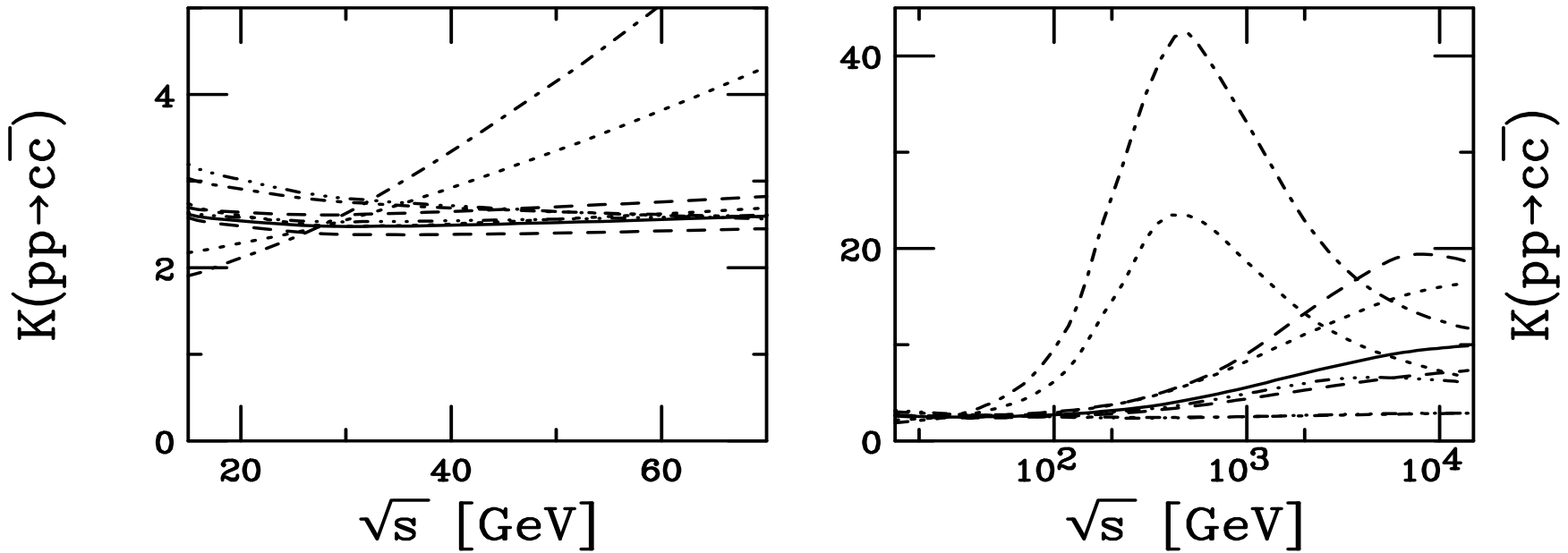

Figure 9: The $c\bar{c}$ K factors calculated using CTEQ6M. The solid curve is the central value $(\mu_F/m, \mu_R/m) = (1, 1)$ with $m = 1.5$ GeV. The upper and lower dashed curves are $m = 1.3$ and 1.7 GeV with $(1,1)$ respectively. The upper and lower dot-dashed curves correspond to $(0.5,0.5)$ and $(2,2)$ while the upper and lower dotted curves are with $(1,0.5)$ and $(0.5,1)$ with $m = 1.5$ GeV.
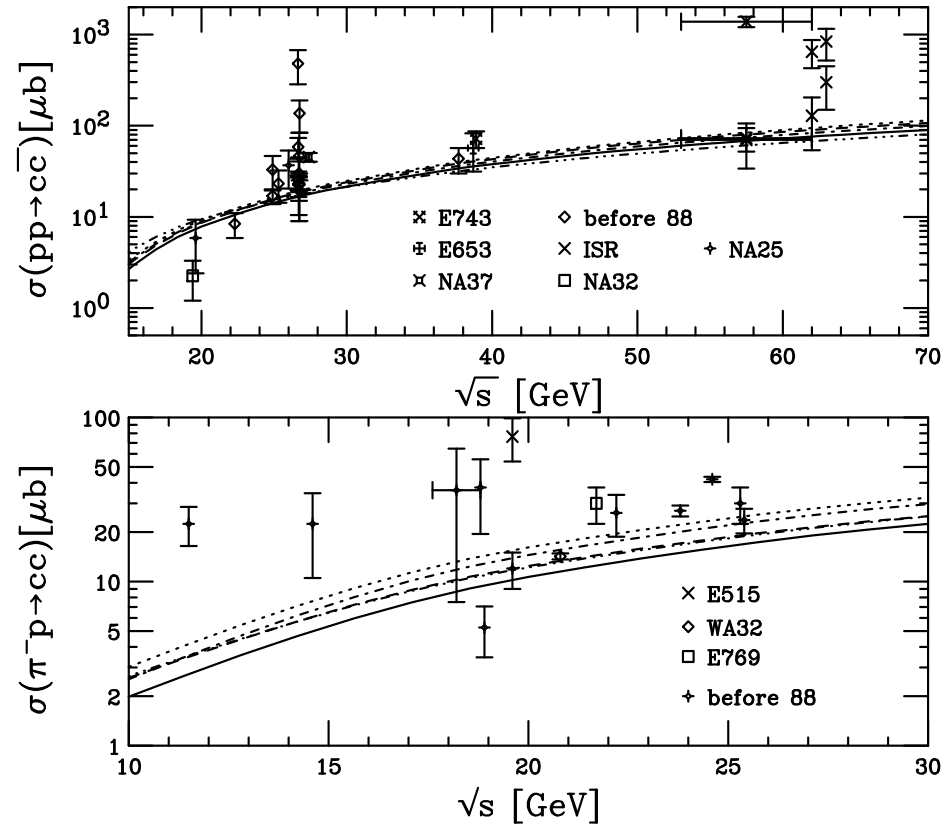
'Best' Agreement Found for Several Cases

Figure 10: Total $c\bar{c}$ cross sections in pp and $\pi^- p$ interactions compared to data. All calculations are fully NLO. The curves are: MRST HO (central gluon) with $\mu = m = 1.4$ GeV (solid) and $\mu = 2m = 2.4$ GeV (dashed); CTEQ 5M with $\mu = m = 1.4$ GeV (dot-dashed) and $\mu = 2m = 2.4$ GeV (dotted); and GRV98 HO with $\mu = m = 1.3$ GeV.

Fitted Fractions and J/ψ Cross Sections in CEM

Case	PDF	m (GeV)	μ/m_T	$\sigma_{J/\psi}/\sigma_C^{\text{CEM}}$
$\psi 1$	MRST HO	1.2	2	0.0144
$\psi 2$	MRST HO	1.4	1	0.0248
$\psi 3$	CTEQ 5M	1.2	2	0.0155
$\psi 4$	GRV 98 HO	1.3	1	0.0229

Table 2: The production fractions obtained from simultaneously fitting F_C to the J/ψ total cross sections and $y = 0$ cross sections as a function of energy. The PDF, charm quark mass, and scales used are obtained from comparison of the $c\bar{c}$ cross section to data.

Case	$\sigma_{J/\psi}^{\text{inc}}$	$\sigma_{J/\psi}^{\text{dir}}$	$\sigma_{\chi c1}$	$\sigma_{\chi c2}$	$\sigma_{\psi'}$
$\psi 1$	2.35	1.46	1.41	2.33	0.33
$\psi 2$	1.76	1.09	1.06	1.74	0.25
$\psi 3$	2.84	1.76	1.70	2.81	0.40
$\psi 4$	2.10	1.31	1.26	2.08	0.29

Table 3: The charmonium cross sections (in μb) for 200 GeV pp collisions. The inclusive and direct J/ψ cross sections are both given.

.

Extrapolated J/ψ Total Cross Sections

Total forward J/ψ cross sections extrapolated to higher energy

Energy dependence obtained from NLO CEM

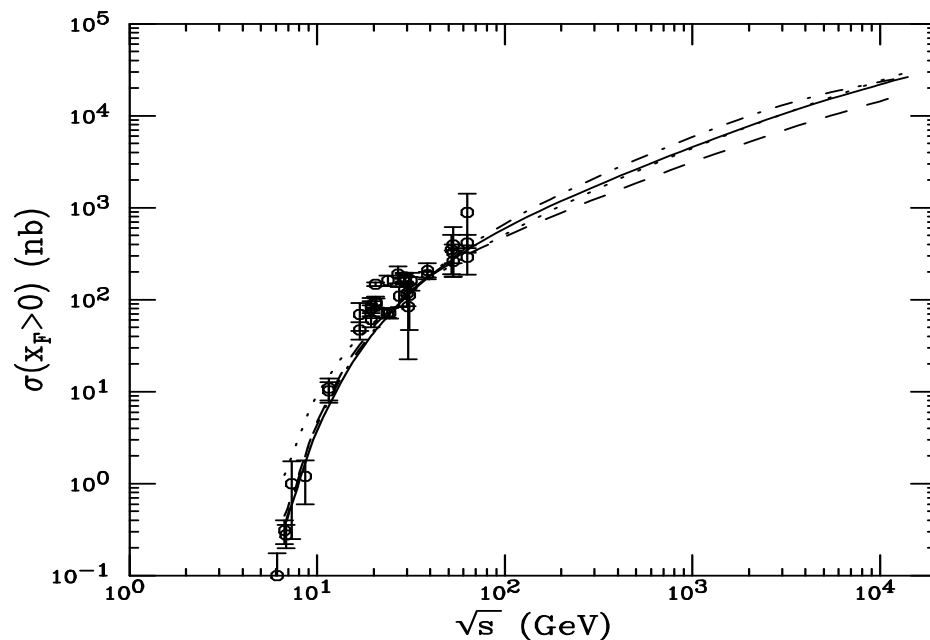Factor of $\sim 1.6-2$ between results at $200\,\text{GeV}$ and at $5.5\,\text{TeV}$

Figure 11: NLO J/ψ forward cross sections. The solid curve employs the MRST HO distributions with $m = 1.2$ GeV $\mu/m_T = 2$, the dashed, MRST HO with $m = 1.4$ GeV $\mu/m_T = 1$, the dot-dashed, CTEQ 5M with $m = 1.2$ GeV $\mu/m_T = 2$, and the dotted, GRV 98 HO with $m = 1.3$ GeV $\mu/m_T = 1$.

From Total Cross Sections to Distributions

Distributions as a function of kinematic variables can provide more information than the total cross section

In total cross section, the quark mass is the only relevant scale

When considering kinematic observables like x_F or p_T, the momentum scale is also relevant so that, instead of $\mu^2 \propto m^2$, one usually uses $\mu^2 \propto m_T^2$ – this difference makes the p_T-integrated total cross section decrease a bit relative to that calculated using the dimensionless scaling functions

Quarkonium p_T distributions at LO for $\mathcal{O}(\alpha_s^3)$ since pair p_T is zero at $\mathcal{O}(\alpha_s^2)$ (LO in total cross section)

Intrinsic transverse momentum added to calculation to reduce steepness of p_T distribution

The Quarkonium p_T Distribution in the $Q\overline{Q}$ NLO Code

.

Gaussian k_T smearing, $\langle k_T^2 \rangle_p = 1$ GeV^2 for fixed target pp and πp, broadened for pA and AA, NLO code adds in final state:

$$g_p(k_T) = \frac{1}{\pi \langle k_T^2 \rangle_p} \exp(-k_T^2/\langle k_T^2 \rangle_p)$$

Comparison with J/ψ and Υ Tevatron data at 1.8 TeV shows that the broadening should increase with energy, to $\langle k_T^2 \rangle_p \approx 2.5$ GeV^2

Fits of increase of $\langle p_T^2 \rangle$ to old data are inadequate to explain this increase so we make a simple linear extrapolation to obtain

$$\langle k_T^2 \rangle_p = 1 + \frac{1}{6} \ln \left(\frac{s}{s_0} \right) \text{ GeV}^2$$

Thus at RHIC energies $\langle k_T^2 \rangle_p = 1.77$ GeV^2 for 200 GeV and 1.38 GeV^2 for 62 GeV pp collisions
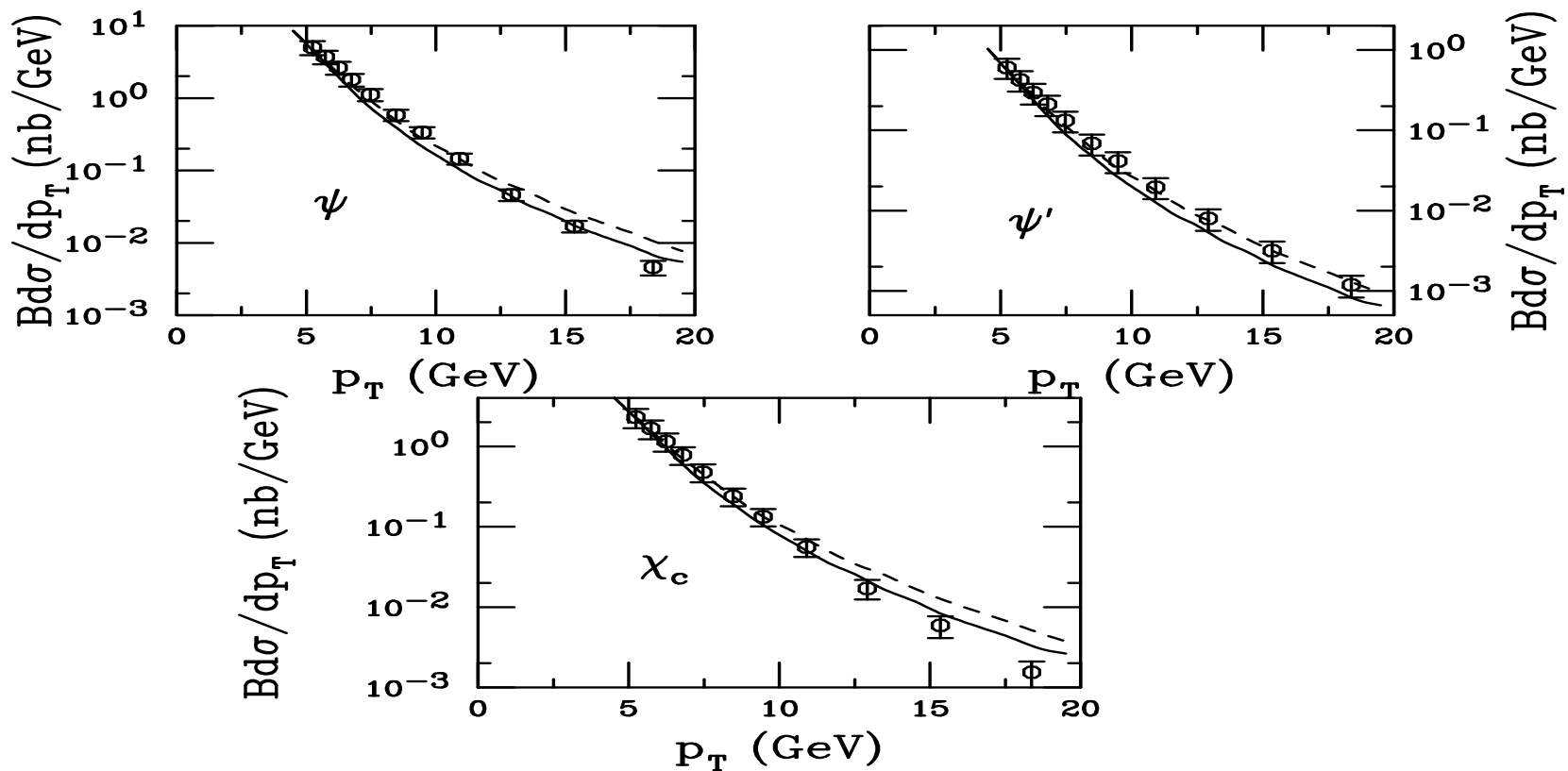
Comparison with Tevatron J/ψ p_T Distributions

Figure 12: The p_T distributions of direct J/ψ as well as J/ψ's from ψ' and χ_c decays calculated for cases $\psi 1$ (solid) and $\psi 4$ (dashed) are compared to the CDF data. We use $\langle k_T^2 \rangle_p = 2.5$ GeV^2.

Nuclear Effects on p_T Broadening

Additional broadening – beyond the intrinsic broadening – assumed to arise from multiple parton scattering in the target before hard interaction

J/ψ, Υ and Drell-Yan show effects of broadening in pA, parameterized as

$$\langle k_T^2 \rangle_{iA} = \langle k_T^2 \rangle_p + (\langle \nu \rangle - 1)\Delta^2(\mu)$$

The broadening is proportional to the average number of collisions of the projectile parton in the target,

$$\langle \nu \rangle = \sigma_{NN} \frac{\int d^2 b T_A^2(b)}{\int d^2 b T_A(b)} = \frac{3}{2}\sigma_{NN}\rho_0 R_A$$

$T_A(b)$ is the nuclear profile function

The second equality is average over impact parameter assuming a spherical nucleus, $\rho_0 = 0.16$ fm^{-3} is the central nuclear density and R_A is the nuclear radius

$\Delta^2(\mu = 2m)$, the strength of the broadening, depends on the scale of the interactions

$$\Delta^2(\mu) = 0.225 \frac{\ln^2(\mu/\text{GeV})}{1 + \ln(\mu/\text{GeV})}\text{GeV}^2$$

	$(\langle \nu \rangle - 1)\Delta^2(\mu)$ (GeV^2)	
$Q\overline{Q}$	pA	central AA
$c\overline{c}$	0.35	0.7
$b\overline{b}$	1.57	3.14

$J/\psi \ p_T$ Distributions at RHIC

At RHIC, $\langle k_T^2 \rangle_p = 1.77 \ \text{GeV}^2$

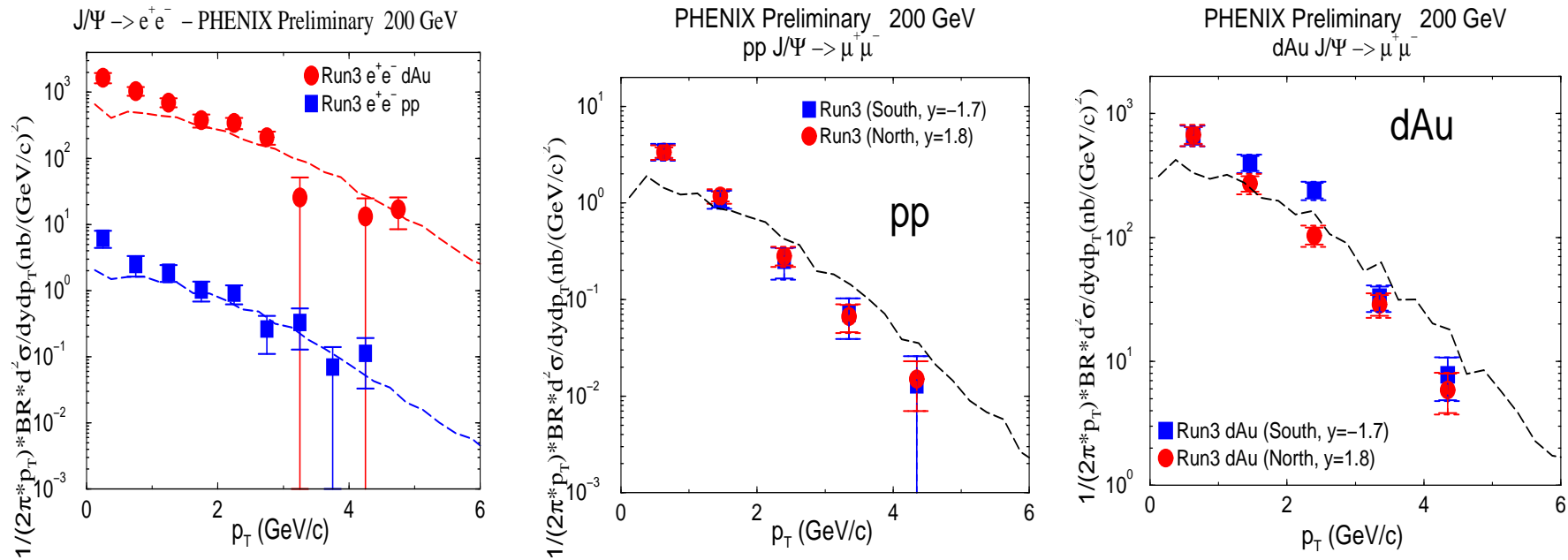Agreement with normalized total cross section good, data somewhat steeper in forward direction than calculation

Figure 13: The inclusive $J/\psi \ p_T$ distributions, calculated for case $\psi 1$, compared to the preliminary PHENIX data. From left to right: e^+e^- pp and d+Au; $\mu^+\mu^-$ pp; and $\mu^+\mu^-$ d+Au. Thanks to Mike Leitch for making these plots!

J/ψ p_T Distributions in AA Collisions

Broadening more effective at 62 GeV since $\langle k_T^2 \rangle_p$ is smaller, 1.38 GeV^2 instead of 1.77 GeV^2 at 200 GeV and average $\langle p_T \rangle$ also smaller (note reduced range of p_T distribution at 62 GeV)

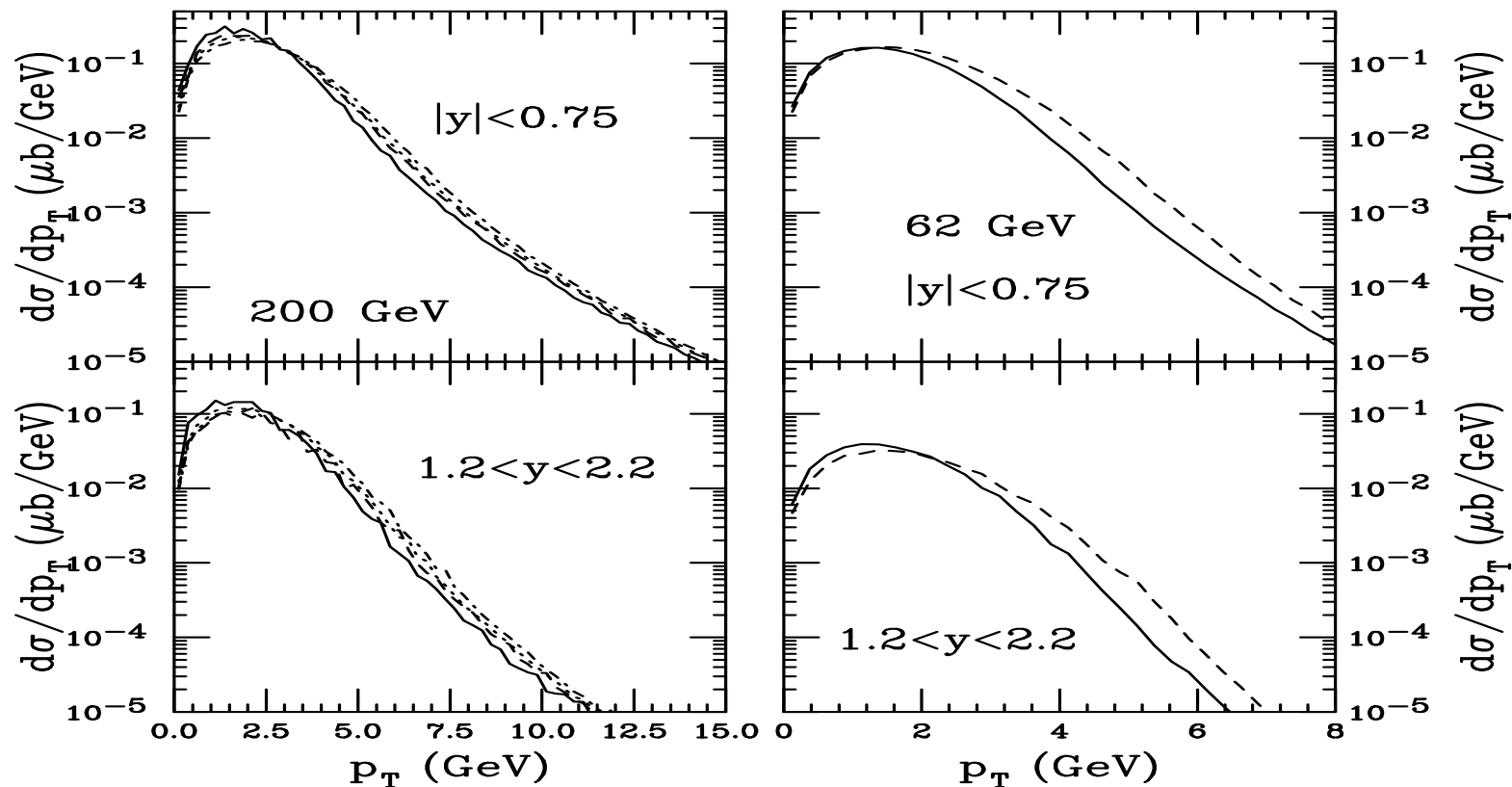Little difference between pp and AA at 200 GeV

Figure 14: The inclusive J/ψ p_T distributions, calculated for case $\psi 1$ for $|y| < 0.75$ (top) and $1.2 < y < 2.2$ (bottom) at $\sqrt{S} = 200$ GeV (left) and 62 GeV (right). At 200 GeV the results show pp (solid), d+Au (dashed), Au+Au (dot-dashed) and Cu+Cu (dotted) interactions. At 62 GeV, we show pp (solid) and Cu+Cu (dashed) results.

Prediction of J/ψ Rapidity Distributions at RHIC

Agreement of CEM calculation with overall normalization of Run 3 data good

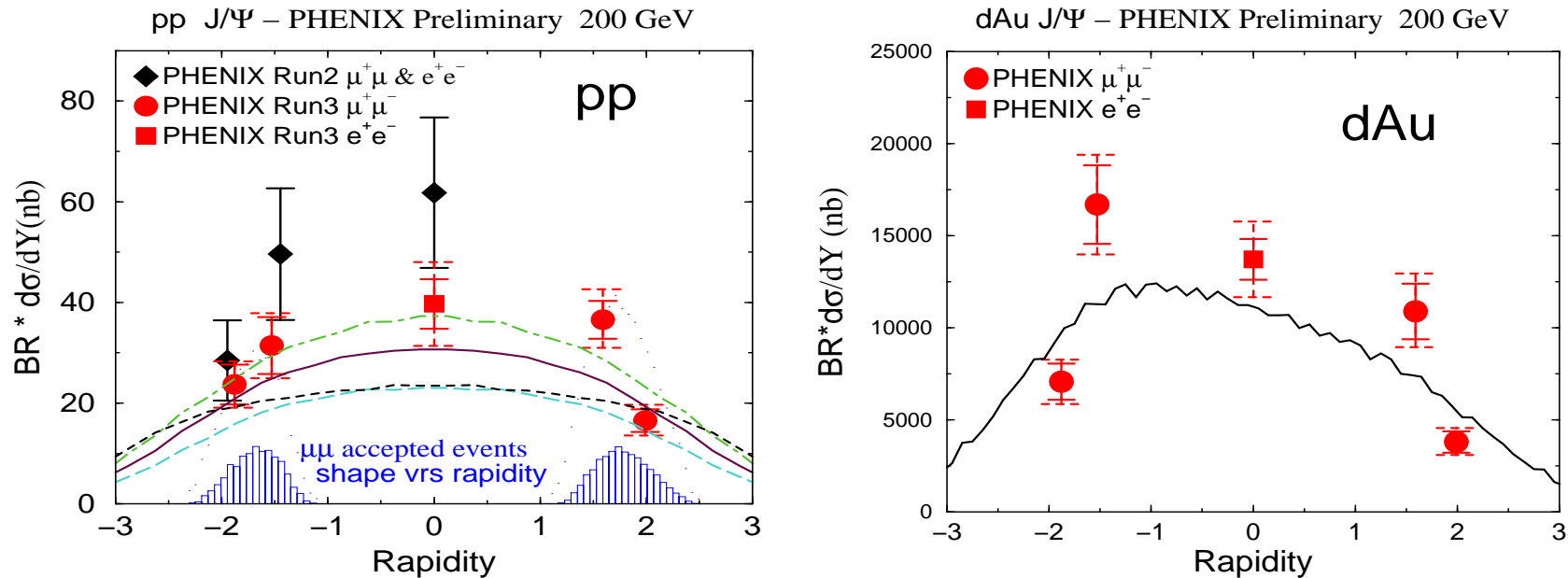Shape has right trend for d+Au with EKS98 shadowing

Figure 15: The inclusive J/ψ y distributions in $\sqrt{s} = 200$ pp (left-hand side for $\psi1$ (solid), $\psi2$ (dashed), $\psi3$ (dot-dashed) and $\psi4$ (dotted)) and d+Au (right-hand side with $\psi1$ and EKS98). The rapidity distributions are unaffected by broadening. Thanks to Mike Leitch for making the plots!

J/ψ Rapidity Distributions in AA Collisions

Note significant antishadowing in Cu+Cu relative to pp at 62 GeV

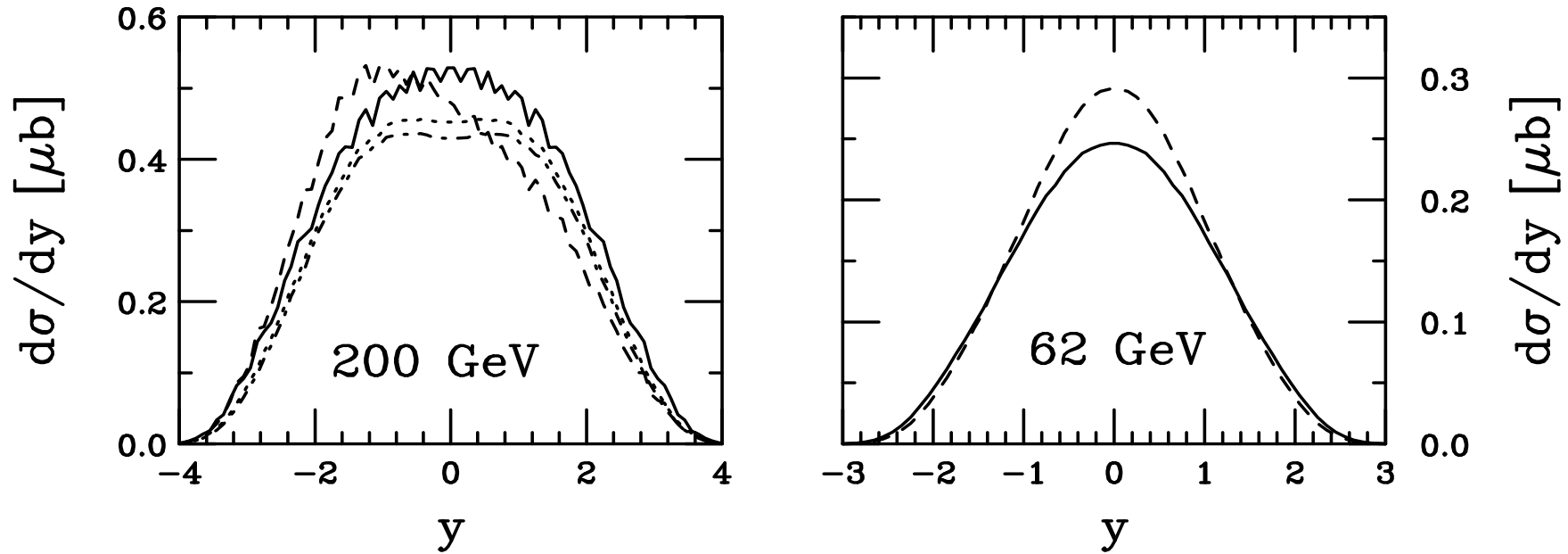At 200 GeV, AA distributions also symmetric around $y = 0$

Figure 16: The inclusive J/ψ y distributions, calculated for case $\psi 1$ at $\sqrt{S} = 200$ GeV (left) and 62 GeV (right). At 200 GeV the results show pp (solid), d+Au (dashed), Au+Au (dot-dashed) and Cu+Cu (dotted) interactions. At 62 GeV, we show pp (solid) and Cu+Cu (dashed) results.

In AB Interactions, Nuclear Effects on Rapidity Distributions Become Important

Nuclear effects seen to be important in charmonium production at fixed target energies

In extrapolated pA cross sections, the exponent α was shown to be a function of both x_F and p_T

Several mechanisms affect A dependence in cold matter, we consider two here:

- Nuclear Shadowing — initial-state effect on the parton distributions affecting the level of production, important as a function of rapidity/x_F

- Absorption — final-state effect, after $c\overline{c}$ that forms the J/ψ has been produced, pair breaks up in matter due to interactions with nucleons

Here we only show effects on charmonium, Υ studies not done yet

Nuclear Parton Distributions

Nuclear parton densities

$$F_i^A(x, Q^2, \vec{r}, z) = \rho_A(s) S^i(A, x, Q^2, \vec{r}, z) f_i^N(x, Q^2) \quad s = \sqrt{b^2 + z^2}$$

$$\rho_A(s) = \rho_0 \frac{1 + \omega(s/R_A)^2}{1 + \exp[(s - R_A)/d]}$$

We use EKS98 and Frankfurt, Guzey and Strikman (FGS) parameterizations: original, FGSo, high, FGSh, and low, FGSl, gluon shadowing

EKS98 has no spatial dependence, two FGS inhomogeneous parameterization recently made available — compare our spatial parameterizations with those of FGS

With no nuclear modifications, $S^i(A, x, Q^2, \vec{r}, z) \equiv 1$.

Spatial dependence of shadowing

Proportional to local nuclear density:

$$S_{\mathrm{WS}}^i = S^i(A, x, Q^2, \vec{r}, z) = 1 + N_{\mathrm{WS}}[S^i(A, x, Q^2) - 1] \frac{\rho(s)}{\rho_0}$$

Proportional to nuclear path length:

$$S_\rho^i(A, x, Q^2, \vec{r}, z) = 1 + N_\rho(S^i(A, x, Q^2) - 1) \frac{\int dz \rho_A(\vec{r}, z)}{\int dz \rho_A(0, z)} \ .$$

Normalization: $(1/A) \int d^2 r dz \rho_A(s) S_{\mathrm{WS}, \rho}^i \equiv S^i$. Larger than average modifications for $b = 0$. Nucleons like free protons when $s \gg R_A$. Similar normalization for FGS inhomogeneous parameterizations.

Comparing Shadowing Parameterizations: x Dependence

Recent parameterizations by Frankfurt *et al* use EKS98 for valence shadowing, stronger gluon shadowing at low x, cuts off modification above $x = 0.25$ for sea, 0.03 for gluon

Newer FGS parameterizations have lower gluon antishadowing, smoother x dependence over $10^{-4} < x < 0.02$
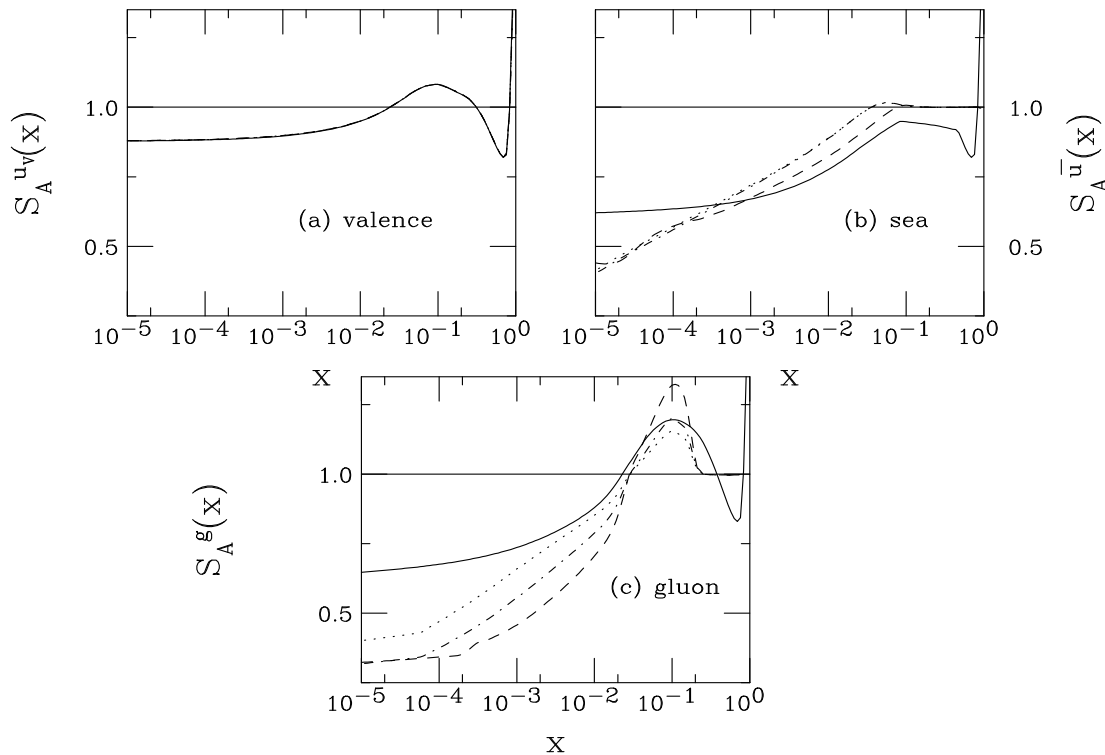
.

Figure 17: The EKS98 and FGS shadowing parameterizations are compared at the scale $\mu = 2m = 2.4$ GeV. The solid curves are the EKS98 parameterization, the dashed, FGSo, dot-dashed, FGSh, dotted, FGSl.

Average x_2 as a Function of Energy and Rapidity

We calculate $\langle x_2 \rangle$ as a function of rapidity in the CEM (N.B. $\langle x_1 \rangle$ is mirror imagine of $\langle x_2 \rangle$)

Increasing $\sqrt{S}$ broadens y range and decreases x_2, at RHIC, $\sqrt{S} = 62$ GeV range is narrower and x_2 values higher than 200 GeV

In PHENIX muon arms, it is possible to reach lower $\langle x_2 \rangle$ than with leading hadrons at similar rapidities: gg dominates and scale is relatively lower
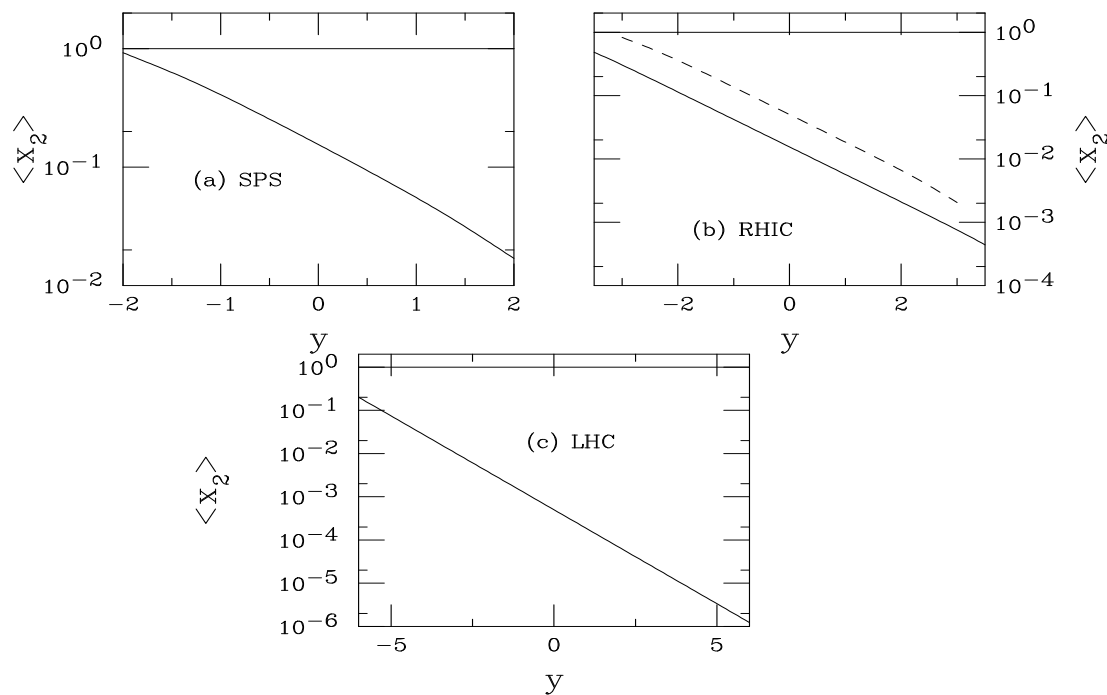

Figure 18: We give the average value of the nucleon momentum fraction, x_2, in pp collisions as a function of rapidity for (a) the CERN SPS with $\sqrt{S} = 19.4$ GeV, (b) RHIC with $\sqrt{S} = 200$ (solid) and 62 (dashed) GeV and (c) the LHC with $\sqrt{S} = 6.2$ TeV.

J/ψ Absorption by Nucleons

Woods-Saxon nuclear density profiles typically used

$$
\begin{aligned}
\sigma_{pA} &= \sigma_{pN} \int d^2b \int_{-\infty}^{\infty} dz\, \rho_A(b,z) S_A^{\text{abs}}(b) \\
&= \sigma_{pN} \int d^2b \int_{-\infty}^{\infty} dz\, \rho_A(b,z) \exp\left\{ -\int_z^{\infty} dz' \rho_A(b,z') \sigma_{\text{abs}}(z'-z) \right\}
\end{aligned}
$$

Note that if $\rho_A = \rho_0$, $\alpha = 1 - 9\sigma_{\text{abs}}/(16\pi r_0^2)$

Absorption models

singlet Individual charmonium cross sections grow quadratically with proper time until formation time; only effective when state can form in target

octet $|(c\bar{c})_8 g\rangle$ state travels through nucleus, only forms charmonium outside; assume either "constant" over all y or "growing", allowing octet to singlet conversion inside target at negative y – little difference at collider energy

NRQCD Nonrelativistic QCD approach differs from CEM in that states are produced with fixed singlet and octet contributions

We show results for absorption of color singlet and color octet states separately in the CEM and a combination of the two in NRQCD

Singlet Absorption Model

All $c\bar{c}$ pairs assumed to be produced in small color singlet states

Assume quadratic growth of cross section with proper time until formation time τ_F (Blaizot and Ollitrault)

Strongest at low to negative x_F where J/ψ can form in the target

Asymptotic ψ' and χ_c cross sections proportional to the final state meson size, *e.g.* $\sigma^{\mathrm{s}}_{\psi'N} = \sigma^{\mathrm{s}}_{J/\psi N}(r_{\psi'}/r_{J/\psi})^2$ (Povh and Hüfner)

$$
\sigma_{\mathrm{abs}}(z'-z) = \begin{cases} \sigma^{\mathrm{s}}_{CN}(\dfrac{\tau}{\tau^C_F})^2 & \text{if } \tau < \tau^C_F \\[2mm] \sigma^{\mathrm{s}}_{CN} & \text{otherwise} \end{cases} .
$$

$$
\begin{aligned}
\tau_F^{J/\psi} &= 0.92 \text{ fm} & \sigma^{\mathrm{s}}_{J/\psi N} &\sim 2.5 \text{ mb} \\
\tau_F^{\psi'} &= 1.5 \text{ fm} & \sigma^{\mathrm{s}}_{\psi'N} &= 3.7\,\sigma^{\mathrm{s}}_{J/\psi N} \\
\tau_F^{\chi_c} &= 2 \text{ fm} & \sigma^{\mathrm{s}}_{\chi_c N} &= 2.4\,\sigma^{\mathrm{s}}_{J/\psi N}
\end{aligned}
$$

Octet Absorption Model

Pre-resonant $c\bar{c}$ pairs travel through the nucleus as $|(c\bar{c})_8 g\rangle$ color octet states

Characteristic octet lifetime $\tau_8 \sim 0.25$ fm

For $x_F \geq -0.1$, path length of $|(c\bar{c})_8 g\rangle$ through the target from its production point is greater than maximum path length

These fast states pass through nucleus in color octets so that the pre-resonant A dependence is the same for J/ψ, ψ' and χ_c (Kharzeev and Satz) — $\sigma_{\text{abs}}^{\text{o}} = 3$ mb agrees with E866 forward A dependence

Universal constant absorption cross section usually assumed for nuclear collision studies (NA38, NA50) where $0 < x_F < 0.18$

At negative x_F, path length is shorter and octet state can neutralize its color inside target and be absorbed as color singlet with 2.5 mb cross section

Only J/ψ likely to be fully formed inside target even though color neutralization may occur for all states

We compare results with no octet to singlet conversion (constant octet) and with conversion (growing octet)

Singlet + Octet Absorption

Relative contributions of singlet and octet production set by NRQCD (Zhang *et al.*)

Equal absorption cross sections for all octet states

Singlet cross sections set by final state size

$$\frac{d\sigma_{pA}^{\psi}}{dx_F} = \int d^2b \left[\frac{d\sigma_{pp}^{\psi,\,\mathrm{oct}}}{dx_F} T_A^{\psi,\mathrm{eff\,(oct)}}(b) + \frac{d\sigma_{pp}^{\psi,\,\mathrm{sing}}}{dx_F} T_A^{\psi,\mathrm{eff\,(sing)}}(b) \right] ,$$

$$\frac{d\sigma_{pA}^{\chi_{cJ}\to J/\psi X}}{dx_F} = \int d^2b \sum_{J=0}^{2} B(\chi_{cJ}\to J/\psi X) \left[\frac{d\sigma_{pp}^{\chi_{cJ},\,\mathrm{oct}}}{dx_F} T_A^{\chi_{cJ},\mathrm{eff\,(oct)}}(b) + \frac{d\sigma_{pp}^{\chi_{cJ},\,\mathrm{sing}}}{dx_F} T_A^{\chi_{cJ},\mathrm{eff\,(sing)}}(b) \right] ,$$

$$\frac{d\sigma_{pA}^{J/\psi,\,\mathrm{tot}}}{dx_F} = \int d^2b \left\{ \left[\frac{d\sigma_{pp}^{J/\psi,\,\mathrm{dir},\,\mathrm{oct}}}{dx_F} T_A^{J/\psi,\mathrm{eff\,(oct)}}(b) \right. \right.$$

$$+ \sum_{J=0}^{2} B(\chi_{cJ}\to J/\psi X) \frac{d\sigma_{pp}^{\chi_{cJ},\,\mathrm{oct}}}{dx_F} T_A^{\chi_{cJ},\mathrm{eff\,(oct)}}(b) + B(\psi'\to\psi X) \frac{d\sigma_{pp}^{\psi',\,\mathrm{oct}}}{dx_F} T_A^{\chi_{cJ},\mathrm{eff\,(oct)}}(b) \Big]$$

$$+ \left[\frac{d\sigma_{pp}^{J/\psi,\,\mathrm{dir},\,\mathrm{sing}}}{dx_F} T_A^{J/\psi,\mathrm{dir},\mathrm{eff\,(sing)}}(b) + \sum_{J=0}^{2} B(\chi_{cJ}\to\psi X) \frac{d\sigma_{pp}^{\chi_{cJ},\,\mathrm{sing}}}{dx_F} T_A^{\chi_{cJ},\,\mathrm{eff\,(sing)}}(b) \right.$$

$$\left. \left. + B(\psi'\to\psi X) \frac{d\sigma_{pp}^{\psi',\,\mathrm{sing}}}{dx_F} T_A^{\psi',\,\mathrm{eff\,(sing)}}(b) \right] \right\}$$

$$T_A^{\mathrm{eff}}(b) = \int_{-\infty}^{\infty} dz\, \rho_A(b,z) \exp\left\{ -\int_z^{\infty} dz'\rho_A(b,z')\sigma_{\mathrm{abs}}(z'-z) \right\}$$

Rapidity Dependence of Homogeneous Absorption

Results shown for different charmonium states: inclusive and direct J/ψ, ψ' and χ_c

Constant and growing octet indistinguishable in detector range, singlet absorption only effective for $y < -1$, NRQCD also shows little rapidity dependence

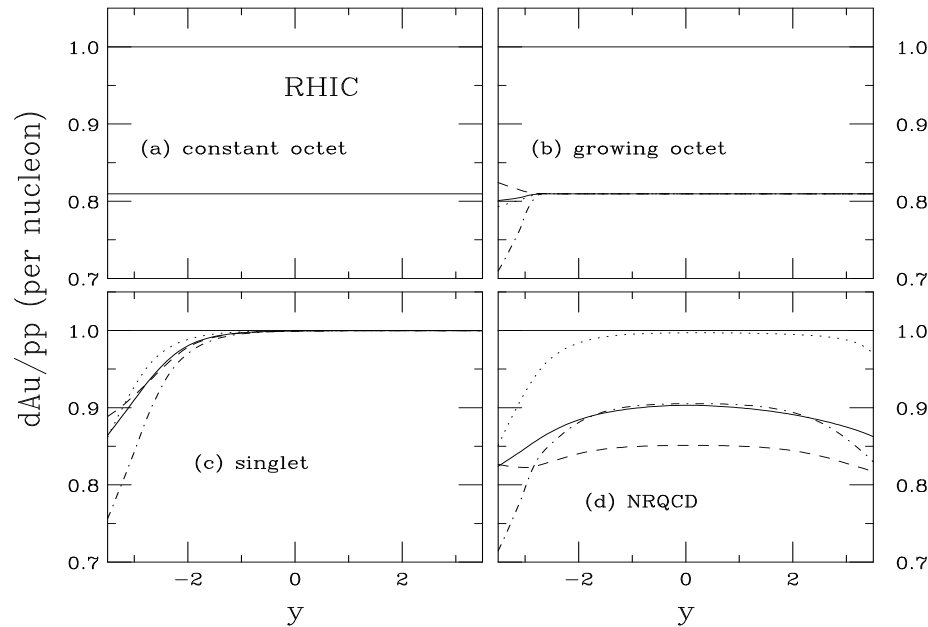Only small effect of growing octet when octet cross section similar to or larger than singlet

Figure 19: The J/ψ dAu/pp ratio at 200 GeV as a function of rapidity for absorption alone. We show (a) constant octet with 3 mb, (b) growing octet with 3 mb asymptotic cross section for all states, (c) singlet with 2.5 mb J/ψ absorption cross section, all calculated in the CEM and (d) NRQCD with a combination of octet and singlet matrix elements. The curves show total J/ψ (solid), direct J/ψ (dashed), ψ' (dot-dashed) and χ_c (dotted).

Effect of Inhomogeneous Absorption

Example of impact parameter dependence of absorption

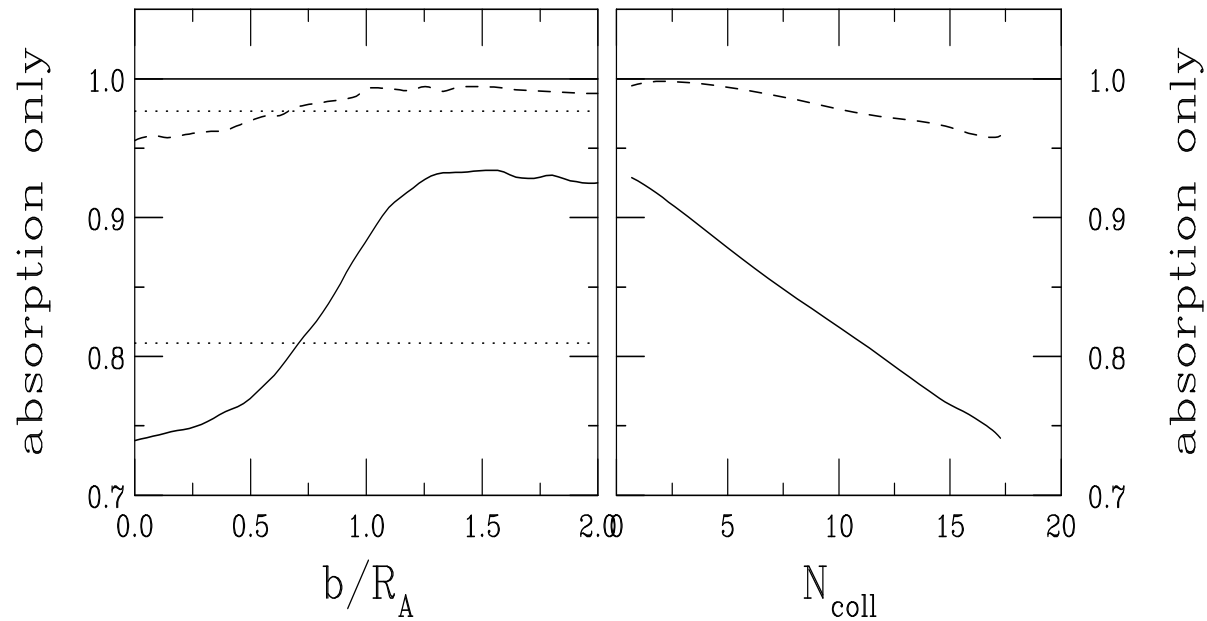Solid curve is 3 mb constant octet cross section, all rapidities, dashed is at $y = -2$, singlet

Figure 20: The J/ψ dAu/pp ratio as a function of b for absorption alone with $\sigma_{\text{abs}} = 3$ mb for a constant octet (all y), solid, and singlet ($y = -2$), dashed. The homogeneous results are indicated by the dotted lines.
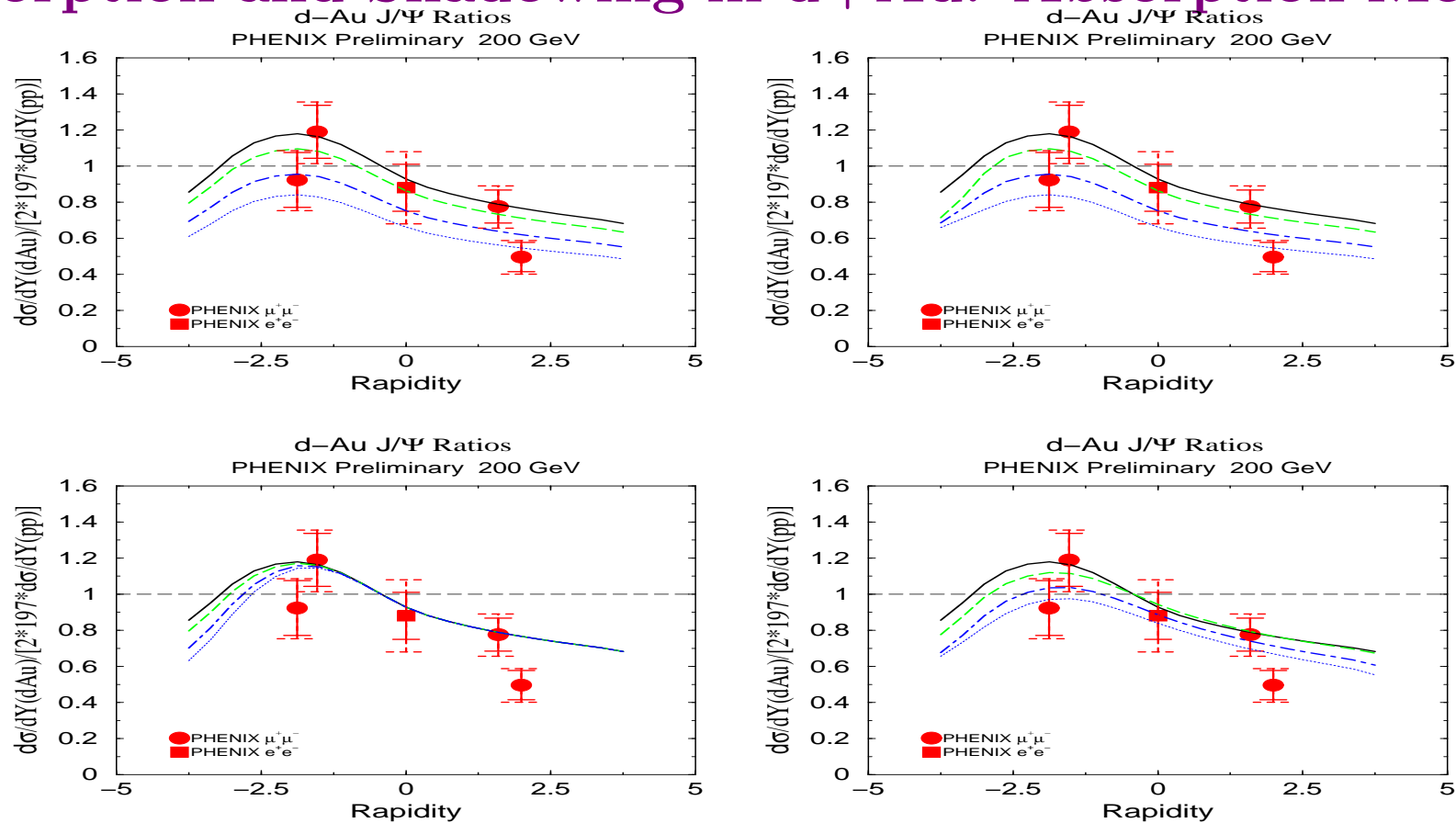
Absorption and Shadowing in d+Au: Absorption Models

Figure 21: The J/ψ dAu/pp ratio at 200 GeV with EKS98 for: (top left) constant octet, (top right) growing octet, (bottom left) singlet and (bottom right) NRQCD. In the first three, we show $\sigma_{abs} = 0$ (solid), 1 (dashed), 3 (dot-dashed) and 5 mb (dotted). For NRQCD, we show no absorption (solid), 1 mb octet/singlet (dashed), 3 mb octet/singlet (dot-dashed), and 5 mb octet/3 mb singlet (dotted).

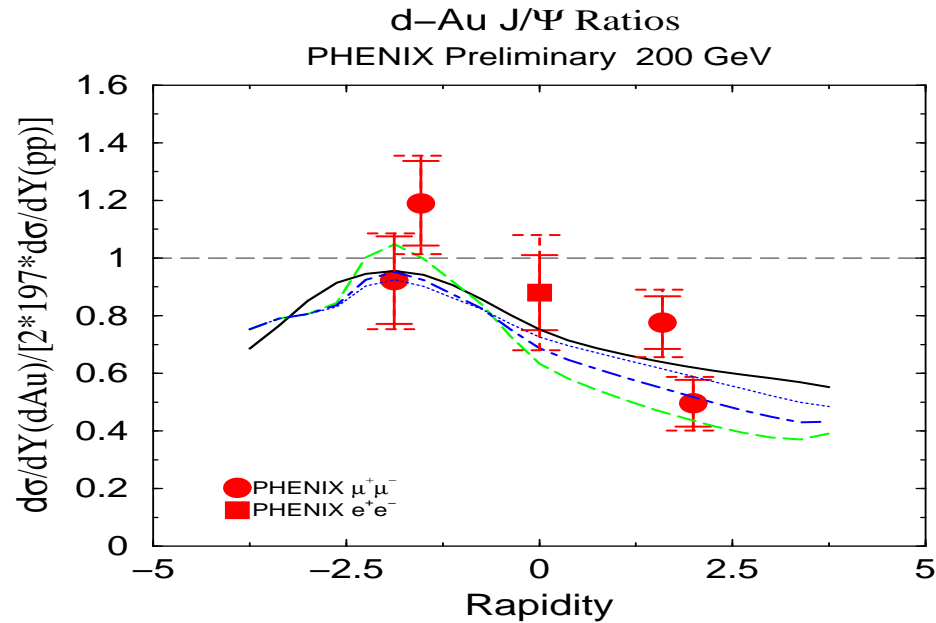# Absorption and Shadowing in d+Au: Shadowing Parameterizations

Figure 22: Comparison of the results for a 3 mb growing octet absorption cross section with the EKS98 (solid), FGSo (dashed), FGSh (dot-dashed) and FGSl (dotted) shadowing parameterizations. Thanks to Mike Leitch for making this plot and all the previous ones for RHIC!

Absorption and Shadowing in 200 GeV Au+Au

Effect of shadowing alone symmetric around $y = 0$, similar to multiplying d+Au/pp ratio by its mirror image, antishadowing peaks at $y \approx \pm 1.5$ are not above unity

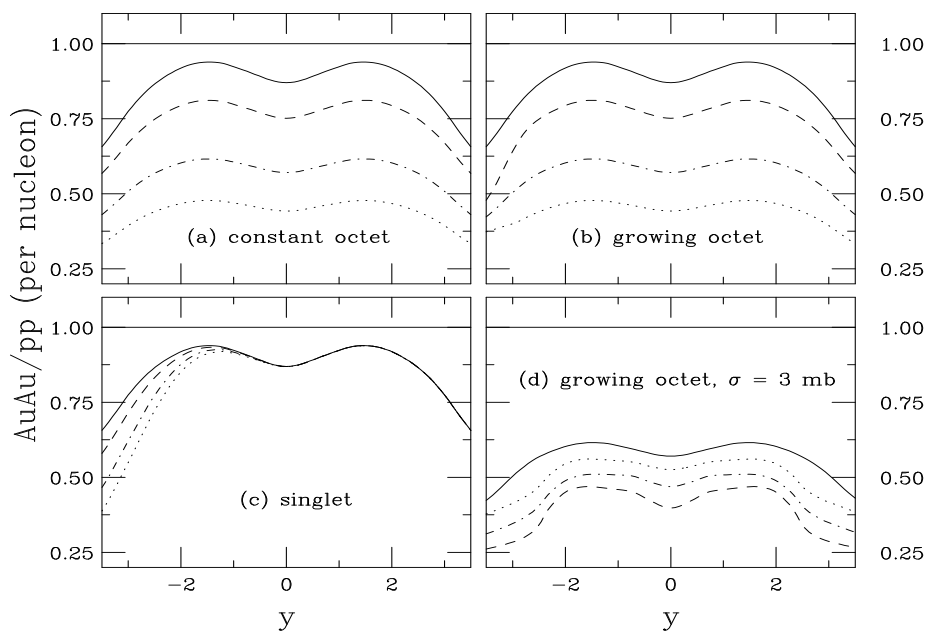Absorption effects stronger when both beams are nuclei, not symmetric around $y = 0$ except for constant octet   .

Figure 23: In (a)-(c) we show the J/ψ AuAu/pp ratio at 200 GeV with the EKS98 shadowing parameterization as a function of rapidity for our absorption models: (a) constant octet, (b) growing octet and (c) singlet. The curves are no absorption (solid), $\sigma_{abs} = 1$ (dashed), 3 (dot-dashed) and 5 mb (dotted). In (d), we compare the results for a 3 mb growing octet absorption cross section with the EKS98 (solid), FGSo (dashed), FGSh (dot-dashed) and FGSl (dotted) shadowing parameterizations.

Absorption and Shadowing in 200 GeV Cu+Cu

Effects similar to Au+Au but weaker due to smaller A

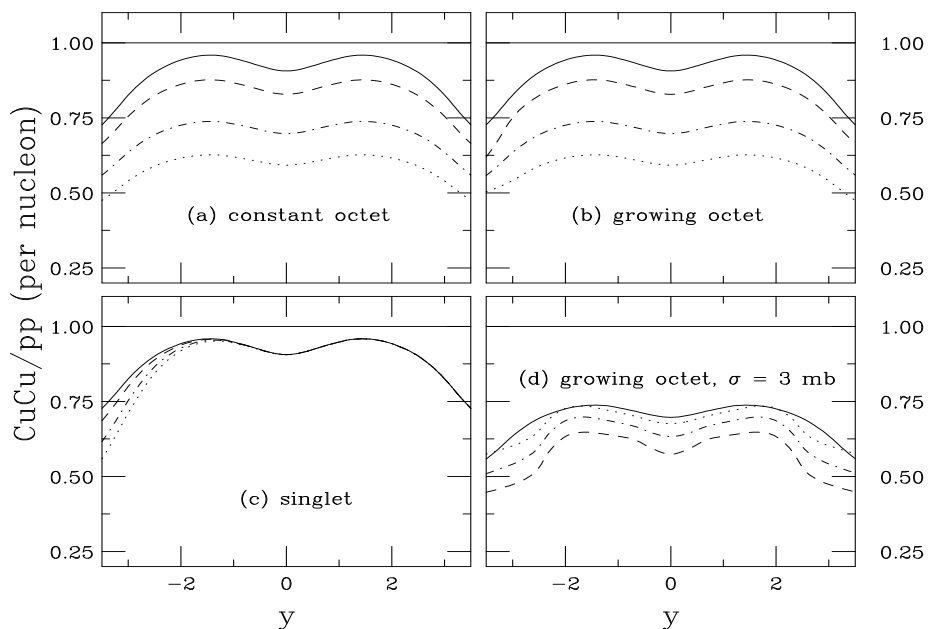FGS parameterizations not available for Cu, used $A = 40$ for these

Figure 24: In (a)-(c) we show the J/ψ CuCu/pp ratio at 200 GeV with the EKS98 shadowing parameterization as a function of rapidity for our absorption models: (a) constant octet, (b) growing octet and (c) singlet. The curves are no absorption (solid), $\sigma_{abs} = 1$ (dashed), 3 (dot-dashed) and 5 mb (dotted). In (d), we compare the results for a 3 mb growing octet absorption cross section with the EKS98 (solid), FGSo (dashed), FGSh (dot-dashed) and FGSl (dotted) shadowing parameterizations.

Absorption and Shadowing in 62 GeV Cu+Cu

Lower energy has $x \approx 0.05$ at $y = 0$, in antishadowing region, gives shadowing peak at $y = 0$

Decrease for $|y| > 0$ due to combination of EMC effect and beginning of shadowing region

Upward turn at large y due to rise after EMC region at large x

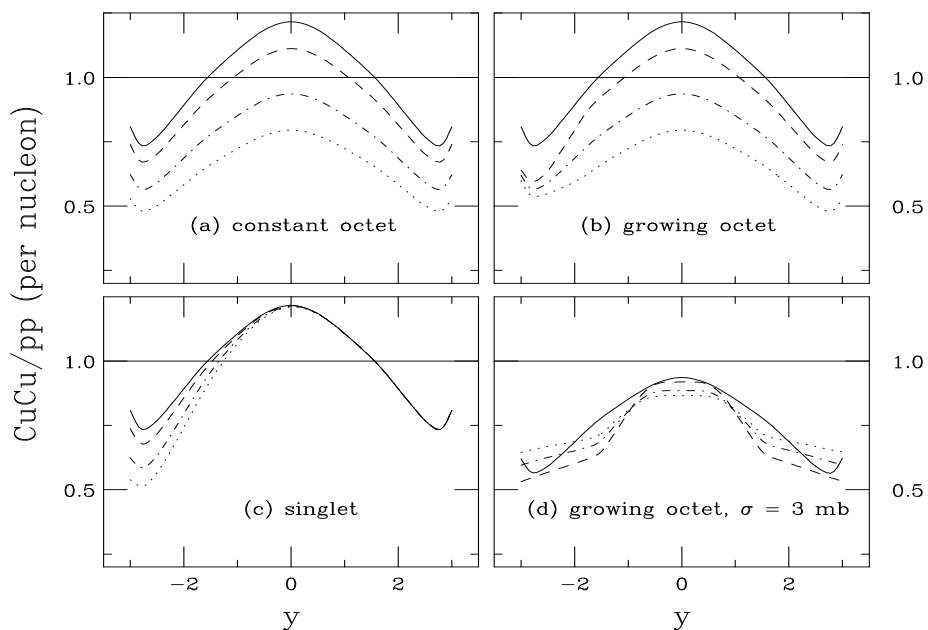Growing octet and singlet absorption effective over larger rapidity range

Figure 25: In (a)-(c) we show the J/ψ AuAu/pp ratio at 200 GeV with the EKS98 shadowing parameterization as a function of rapidity for our absorption models: (a) constant octet, (b) growing octet and (c) singlet. The curves are no absorption (solid), $\sigma_{abs} = 1$ (dashed), 3 (dot-dashed) and 5 mb (dotted). In (d), we compare the results for a 3 mb growing octet absorption cross section with the EKS98 (solid), FGSo (dashed), FGSh (dot-dashed) and FGSl (dotted) shadowing parameterizations.

41

Inhomogeneous Shadowing and Absorption in d+Au

PHENIX results presented as a function of N_{coll}, the convolution of the nuclear profile functions multiplied by the inelastic NN cross section, 42 mb at RHIC

$$N_{\text{coll}}(b) = \sigma_{NN}^{\text{in}} \int d^2 s T_A(s) T_B(|\vec{b} - \vec{s}|)$$

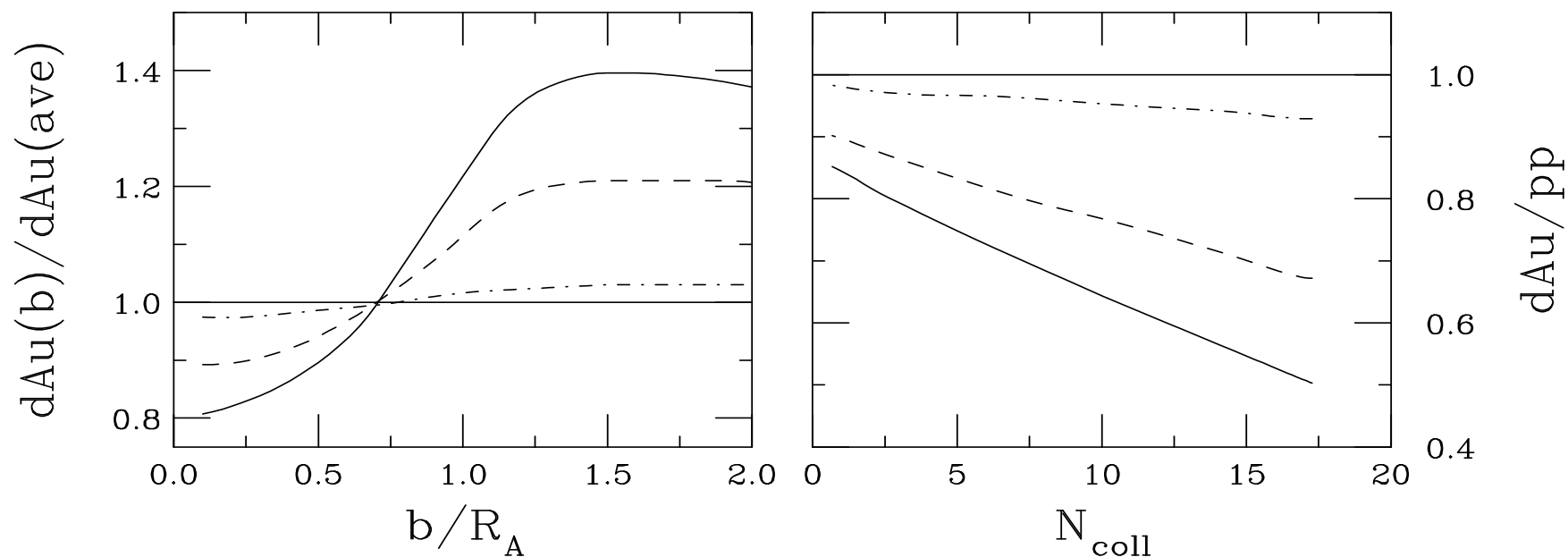Results with EKS98 compared at $y = -2$ (antishadowing), 0 (transition region) 2 (shadowing)

Figure 26: Left-hand side: The J/ψ ratio $(\text{dAu}(b)/pp)/(\text{dAu}(\text{ave})/pp)$ as a function of b/R_A. Right-hand side: The ratio dAu/pp as a function of N_{coll}. Results are shown for $y = -2$ (dot-dashed), $y = 0$ (dashed) and $y = 2$ (solid) at 200 GeV for a growing octet with $\sigma_{\text{abs}} = 3$ mb and the EKS98 parameterization.

Comparison of N_{coll} Dependence in d+Au

Path length parameterization,$S_{\mathrm{P},\rho}$, with EKS98 and FGSo gives linear N_{coll} dependence due to long tails of density distributions

FGSh and FGSl forced to $S = 1$ at $b = 10$ fm so that as $N_{\mathrm{coll}} \rightarrow 1$, shadowing disappears and only residual absorption remains   .
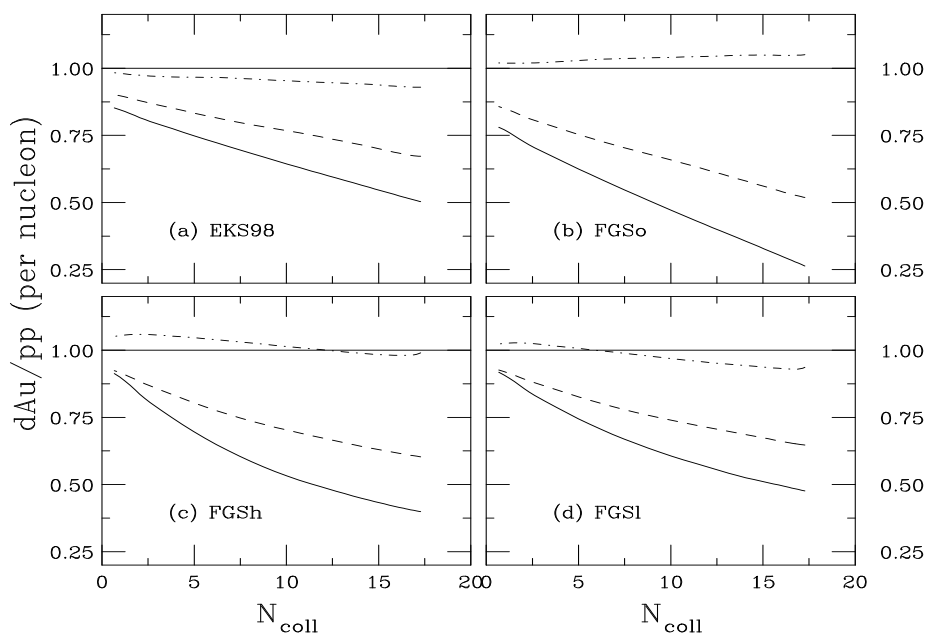

Figure 27: The ratio dAu/pp as a function of N_{coll} for the EKS98 (a), FGSo (b), FGSh (c) and FGSl (d) shadowing parameterizations. The calculations with EKS98 and FGSo use the inhomogeneous path length parameterization while that obtained by FGS is used with FGSh and FGSl. Results are given for $y = -2$ (dot-dashed), $y = 0$ (dashed) and $y = 2$ (solid) at 200 GeV for a growing octet with $\sigma_{\mathrm{abs}} = 3$ mb.

Prediction of N_{coll} Dependence in Au+Au

In nucleus-nucleus collisions, we only show $y = 0$ and 2 since, for a growing octet, the results at $y = 2$ and -2 are symmetric

$N_{\text{coll}} > 1$ for $b < 2R_A$ so FGSh and FGSl does not change as fast with N_{coll} as in d+Au

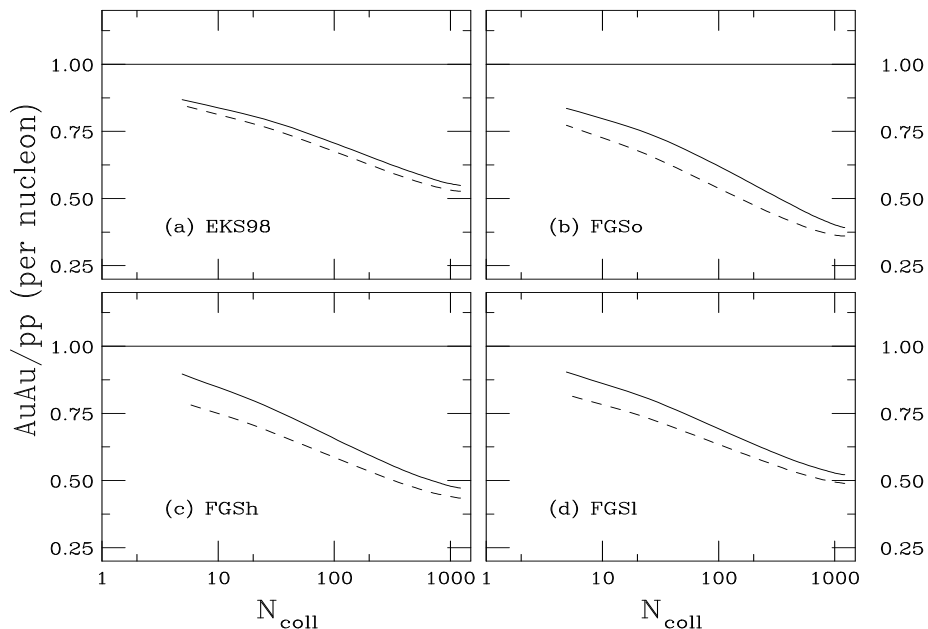Result with $y = 0$ lower than for $y = 2$ due to "dip" between peaks seen in homogeneous calculations

.

Figure 28: The ratio AuAu/pp as a function of N_{coll} for the EKS98 (a), FGSo (b), FGSh (c) and FGSl (d) shadowing parameterizations. The calculations with EKS98 and FGSo use the inhomogeneous path length parameterization while that obtained by FGS is used with FGSh and FGSl. Results are given for $y = 0$ (dashed) and $y = 2$ (solid) at 200 GeV for a growing octet with $\sigma_{\text{abs}} = 3$ mb.

Prediction of N_{coll} Dependence in 200 GeV Cu+Cu Collisions

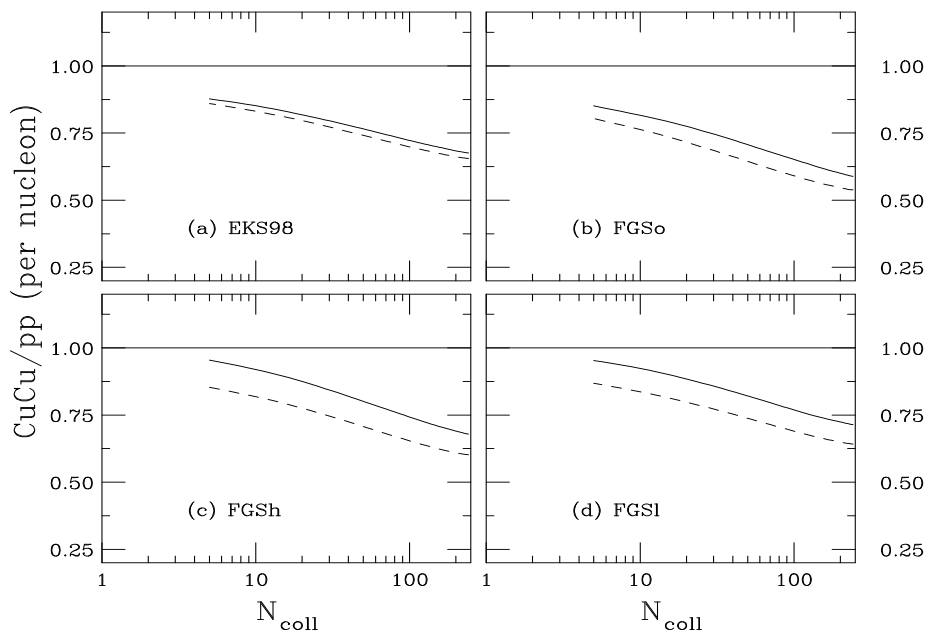N_{coll} lower for Cu+Cu due to smaller nuclear size

Figure 29: The ratio CuCu/pp as a function of N_{coll} for the EKS98 (a), FGSo (b), FGSh (c) and FGSl (d) shadowing parameterizations. The calculations with EKS98 and FGSo use the inhomogeneous path length parameterization while that obtained by FGS is used with FGSh and FGSl. Results are given for $y = 0$ (dashed) and $y = 2$ (solid) at 200 GeV for a growing octet with $\sigma_{\text{abs}} = 3$ mb.

Prediction of N_{coll} Dependence in 62 GeV Cu+Cu Collisions

At $\sqrt{S} = 62$ GeV, number of collisions reduced because $\sigma_{NN}^{\mathrm{in}}$ is smaller at the lower energy

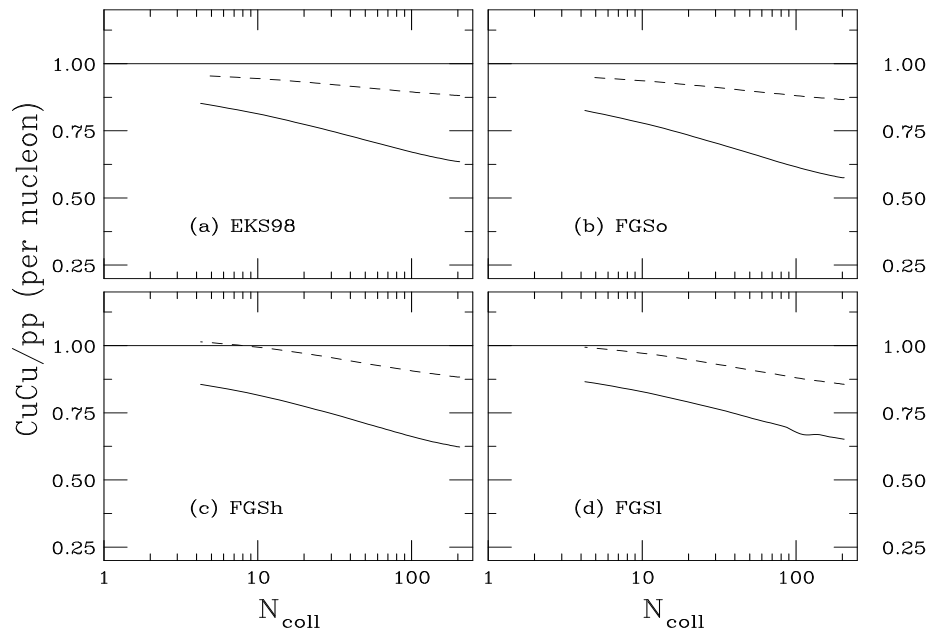Now, due to different shapes of the shadowing results with energy, the $y = 0$ curve is again above that of $y = 2$.

Figure 30: The ratio CuCu/pp as a function of N_{coll} for the EKS98 (a), FGSo (b), FGSh (c) and FGSl (d) shadowing parameterizations. The calculations with EKS98 and FGSo use the inhomogeneous path length parameterization while that obtained by FGS is used with FGSh and FGSl. Results are given for $y = 0$ (dashed) and $y = 2$ (solid) at 62 GeV for a growing octet with $\sigma_{\mathrm{abs}} = 3$ mb.

Summary .

- CEM gives good agreement with hadroproduction results, even for p_T distributions, without K factors .

- We used d+Au calculations at 200 GeV to extrapolate shadowing and absorption baseline for AA collisions .

- Intrinsic k_T broadening important for p_T distributions, nuclear effects on broadening are larger at 62 GeV than at 200 GeV .

- $c\bar{c}$ production could be used as baseline for J/ψ effects in AA but care must be taken in comparing total charm cross sections – need to have better measurements to higher p_T